AIAA 2002-2743
Boundary Layer Transition On Slender Cones In Conventional And Low Disturbance Mach 6 Wind Tunnels

Thomas J. Horvath, Scott A. Berry, Brian R. Hollis,
Chau-Lyan Chang, and Bart A. Singer
NASA Langley Research Center
Hampton, VA 23681-2199

32nd AIAA Fluid Dynamics Conference and Exhibit
June 24-27, 2002
St. Louis, Missouri

BOUNDARY LAYER TRANSITION ON SLENDER CONES IN CONVENTIONAL AND LOW DISTURBANCE MACH 6 WIND TUNNELS

Thomas J. Horvath*, Scott A. Berry*, Brian R. Hollis*⊕
Chau-Lyan Chang†⊕, and Bart A. Singer†⊕
NASA Langley Research Center

Abstract

An experimental investigation was conducted on a 5-degree half-angle cone and a 5-degree half-angle flared cone in a conventional Mach 6 wind tunnel to examine the effects of facility noise on boundary layer transition. The influence of tunnel noise was inferred by comparing transition onset locations determined from the present test to that previously obtained in a Mach 6 low disturbance quiet tunnel. Together, the two sets of experiments are believed to represent the first direct comparison of transition onset between a conventional and a low disturbance wind tunnel using a common test model and transition detection technique. In the present conventional hypersonic tunnel experiment, separate measurements of heat transfer and adiabatic wall temperatures were obtained on the conical models at small angles of attack over a range of Reynolds numbers, which resulted in laminar, transitional, and turbulent flow. Smooth model turbulent heating distributions are compared to that obtained with transition forced via discrete surface roughness. The model nosetip radius was varied to examine the effects of bluntness on transition onset. Despite wall-to-total temperature differences between the transient heating measurements and the adiabatic wall temperature measurements, the two methods for determining sharp cone transition onset generally yielded equivalent locations. In the "noisy" mode of the hypersonic low disturbance tunnel, transition onset occurred earlier than that measured in the conventional hypersonic tunnel, suggesting higher levels of freestream acoustic radiation relative to the conventional tunnel. At comparable freestream conditions, the transition onset Reynolds number under low disturbance conditions was a factor of 1.3 greater than that measured on flared cone in the LaRC conventional hypersonic tunnel and a factor of 1.6 greater than the flared cone run in the low disturbance tunnel run "noisy". Navier-Stokes mean flow computations and linear stability analysis were conducted to assess the experimental results and have indicated N factors associated with sharp flared cone transition onset to be approximately a factor of 2 lower than that inferred from the corresponding low disturbance tunnel measurements.

Nomenclature

h	heat transfer coeff. (lbm/ft^2-sec), $q/(H_{aw}- H_w)$ where $H_{aw} = H_{t,2}$
H	enthalpy (BTU/lbm)
k	boundary layer trip height (in.)
L	reference length based on sharp tip model (in)
M	Mach number
N	exponential factor in amplification ratio e^N from linear stability theory
P	pressure, psia
q	heat transfer rate (BTU/ft^2-sec)
R or r	radius (in.)
t	time (sec)
Re	unit Reynolds number (1/ft)
T	temperature (°F)
x	axial distance from cone apex (in.)
α	angle of attack (degree)
ϕ	roll angle (degree)
δ	boundary layer height (in.)
θ_c	cone half angle (degree)

Subscripts

aw	adiabatic wall
B	blunted nosetip
b	base
e	local value at boundary layer edge
n	model nose
ref	Fay and Riddell stag. heating (R_n=0.125-in.)
S	sharp nosetip
T	transition onset
o	reservoir conditions
2	stagnation conditions behind normal shock
∞	free-stream conditions
w	wall

Introduction

Thermal effects resulting from boundary layer transition during hypersonic ascent, cruise, or entry can represent an important thermal protection system (TPS) design constraint[1]. From a thermal protection perspective, the success of the ceramic-based tiles utilized on the US shuttle orbiter was in some regards the consequence of a conservative (and costly) design philosophy. Strategies for achieving an economically viable next generation space transportation system with

*Aerothermodynamics Branch, NASA Langley Research Center, Hampton, VA.

† Computational, Modeling & Simulation Branch, NASA Langley Research Center, Hampton, VA.

⊕ Member, AIAA

an emphasis on risk reduction and enhanced crew safety may include refined or alternative TPS concepts. From an operations perspective, it has been suggested that metallic TPS may offer more durability at reduced cost. Relative to ceramic TPS however, the thermal limitations of current metallic systems impose trajectory tailoring requirements in order to delay transition to as low a Mach number as possible; this is to reduce the probability that turbulent heating levels do not exceed the peak levels experienced during the laminar phase of entry[2]. With the shuttle orbiter, boundary layer transition concerns are primarily associated with re-entry. The designer of an extended cruise hypersonic air breather faces additional transition challenges. Uncertainties in drag prediction[3] and propulsion system efficiencies[4] (e.g. inlet mass capture, fuel mixing) resulting from the presence or absence of boundary layer transition could impact vehicle and mission performance.

Until a credible mechanism based[5] approach to transition prediction is developed, the TPS designer will continue to rely on prediction strategies that include empirical methods derived from ground based measurements. Wind tunnel based boundary layer transition criteria are usually considered conservative due to influences of facility disturbances which presumably cause transition to occur at lower values of Reynolds numbers than may actually occur in flight[5]. Quiet wind tunnel technologies developed at and incorporated into supersonic and hypersonic wind tunnels at the NASA LaRC in the 1980's and 1990's have clearly established the influences of noise on transition and have advanced the understanding of transition via stability experiments conducted in these facilities[6-27] as well as in conventional tunnels[28-32]. Despite advances in quiet wind tunnel technology, relatively few low disturbance supersonic or hypersonic facilities exist. Those operational today are typically deficient in Reynolds number relative to representative flight conditions and are generally not operated in a manner conducive for fast paced aeroheating configuration assessment/screening studies. Thus, despite recognized limitations, conventional hypersonic facilities such as the NASA LaRC 20-Inch Mach 6 Air Tunnel continue to serve as the primary source for experimental data[33-46] from which to develop empirical methods for flight transition prediction.

The purpose of this paper was to qualitatively assess the acoustic disturbance environment of the NASA LaRC 20-Inch Mach 6 Air Tunnel; characterize facility noise effects on parametric trends associated with hypersonic slender body transition; and aid in the interpretation of transition criteria developed from data obtained in a conventional hypersonic tunnel. The relative disturbance environment of this conventional tunnel was deduced via differences in smooth wall transition onset locations measured on two conical models previously tested in the LaRC Mach 6 Nozzle Test Chamber (NTC) Quiet Tunnel[11-24]. In addition, spectra associated with the tunnel freestream fluctuations were made with an uncalibrated hotwire. While the disturbance growth within the boundary layer of the wind tunnel models was not measured at this time (as in a stability experiment), the two sets of experiments are believed to represent the first direct comparison of transition onset between a conventional and a low disturbance hypersonic wind tunnel operated at both high and low noise environments using common models at comparable freestream conditions. This direct comparison has important implications as the effects of acoustic noise on transition onset are often determined by operating the low disturbance facility in a "noisy" mode[5-10, 17] (diverter valves normally open to promote a laminar nozzle wall boundary layer are closed, resulting in a turbulent nozzle boundary layer). Although it has been suggested that this "noisy" mode would likely produce higher levels of acoustic radiation relative to a conventional tunnel the potential effect has never been quantified (via comparative testing of models used in quiet tunnel research in a conventional facility). Also, as noted in Ref. 5, a supersonic low disturbance environment has produced trends in transition onset (e.g. bluntness or angle of attack effects) that have been different to that observed when the same facility is run "noisy". This study presented an opportunity from which to compare trends in slender body *hypersonic* transition under conventional tunnel conditions with those found s*upersonically* under high and low noise conditions (measurements to identify parametric trends at low and high disturbance levels were never attempted in the Mach 6 NTC Quiet Tunnel).

In the present conventional hypersonic tunnel experiment, two measurement techniques (separate wind tunnel runs) were used to identify transition onset. Measurements of heat transfer rate and adiabatic wall temperatures were obtained independently on the cone models at small angles of attack over a range of length Reynolds numbers ($0.8x10^6$ to $16x10^6$) that resulted in laminar and turbulent flow. Wall-to-total temperature ratio for the laminar heating measurements and the laminar adiabatic wall temperature measurements were 0.59 and 0.86, respectively. Nosetip bluntness ($0.0001< R_n <0.125$-inch) and angle of attack ($\pm$ 0, 0.5, 1, 2, 4, 4.5 degree) effects on transition were obtained to compliment experimental investigations on similar slender cones that were tested in conventional hypersonic tunnels[47-56], as well as cones tested in a low disturbance supersonic tunnel[7-10]. Correlation of measured transition onset locations with linear stability theory has been made. The evolution of the smooth wall surface heating from a laminar to a transitional and turbulent state are compared to those obtained with transition forced via discrete surface roughness.

Characterization of the heating on complex shapes and quantifying the effects of surface roughness in terms of correlations derived from conventional ground based

testing will continue into the near future. Most of the NASA's recently proposed X-vehicles have been tested in the NASA LaRC 20-Inch Mach 6 Air Tunnel with a majority of the aerothermodynamic studies emphasizing hypersonic transition and the characterization of surface roughness effects[33-46]. While it is recognized that improvements in TPS technology have been made since the first flight of the US shuttle orbiter, most have not been flight demonstrated. A recent review of roughness-dominated transition suggests TPS technology for reentry vehicles in the near future may continue to be roughness dominated[57]. Traditional ceramic TPS tiles such as those used on the Shuttle Orbiter often suffer launch-induced damage and/or develop protruding gap fillers. Both forms of local surface roughness have been responsible for the occurrence of early boundary layer transition in flight[58]. Stitching patterns found on thermal blankets produce another form of local roughness. Metallic TPS panels that were proposed for use on the X-33[33,59-60] could have been susceptible to thermally induced expansion/bowing producing roughness in the form of a wavy wall.

It is generally accepted that boundary layer transition can result from parametric instabilities, mode interactions, or transition bypass mechanisms (a term commonly used to identify transition modes which bypass the linear growth process of disturbances). When vehicle surface roughness are present (a typical bypass), it is believed that facility noise from conventional tunnels has little effect on transition. Experimental studies have suggested that while noise may have little effect for roughness heights large enough to be considered effective[61] (turbulence initiated immediately downstream of the roughness element site), there still may be an influence of wind tunnel noise on transition onset data derived from roughness that are less than effective[62-63]. Based upon experimental evidence suggesting the susceptibility of less than effective roughness elements to acoustic disturbances, quantification of the conventional facility disturbance environment is essential.

Experimental Methods

Models

The present tests in the LaRC 20-Inch Mach 6 Air Tunnel utilized two models that were originally constructed for testing in the LaRC Mach 6 NTC Quiet Tunnel. The original stability experiments were to be conducted on a 25-inch long (sharp tip) 5-degree straight cone model shown schematically in Fig. 1a. Undocumented surface temperature measurements made on the 5-degree straight cone in the LaRC Mach 6 NTC Quiet Tunnel revealed that boundary layer transition onset did not occur.

Consequently, the emphasis of the stability tests shifted to the second conical model (with a flared base). The purpose of the flare was to promote boundary layer instability via an adverse pressure gradient to insure transition would occur on the model within the limited quiet flow Reynolds number capability of the Mach 6 NTC Quiet Tunnel.

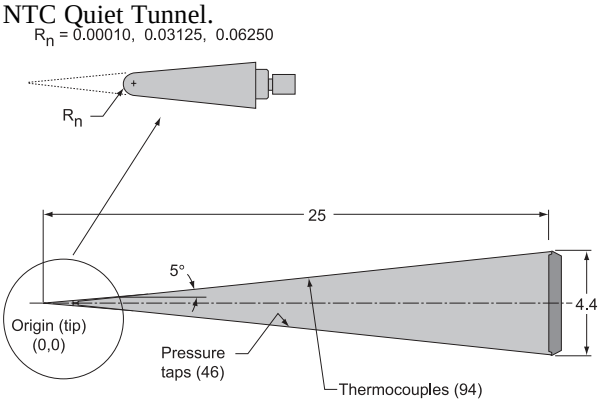

(a) 5 deg straight cone and nosetip dimensions (inches)

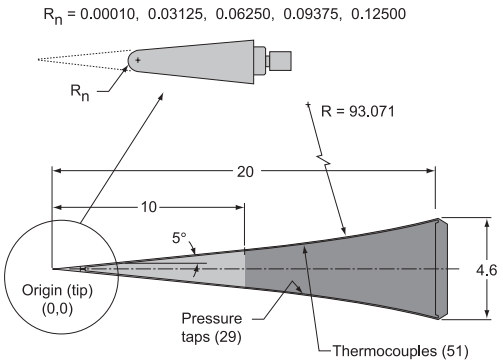

(b) 5 deg flared cone (Model 93-10) and nosetip dimensions (inches)

Fig. 1. Schematic diagram of slender cone models.

A schematic diagram of the flared cone model geometry is shown in Fig. 1b. Measuring 20-inches in length (sharp tip) the model base diameter is 4.6-inch. The first 10-inch section of the model consists of a 5-degree half angle cone followed by a 10-inch section comprised of an outward flare. Tangency was specified at the cone/flare junction. An arc radius of 93.07-inches defined the flare curvature. Details of the 5-degree half angle flared cone model (designation 93-10) can be found in Ref. 16.

Both models were constructed thin walls fabricated from 15-5 stainless steel to reduce surface heat conduction effects and to bring the models to thermal equilibrium as quickly as possible during a run. The flared cone model was constructed with five interchangeable nosetips (R_n= 0.0001, 0.03125, 0.06250, 0.09375, and 0.125-inch) fabricated from 13-8 stainless steel (see Fig. 1a-b) while the straight cone had three nosetips (R_n= 0.0001, 0.03125, 0.06250). The surface finish on both models was originally highly polished to minimize waviness and roughness induced

effects on boundary layer stability and, for the present test, appeared to be free of large surface scratches (despite several entries into the quiet tunnel and the subsequent long-term storage).

Discrete and distributed surface roughness were utilized to force boundary layer transition to compare against smooth body transition and to insure fully turbulent flows were obtained in the present study. Photographs of the boundary layer trips are shown in the inset of Fig. 2. Discrete roughness elements (of diamond planform shape) used in this study were originally conceived to simulate a raised shuttle TPS tile as described in Ref. 33. Individual roughness elements (0.050 x 0.050-in.) were fabricated from adhesively backed teflon tape of various thickness (k= 0.0045, 0.0065, 0.0115-in.). The roughness element was applied to the model surface at various axial locations (x/L= 0.1, 0.2, and 0.4) along the array of thermocouples. In addition, discrete and distributed (randomly dispersed) surface roughness in the form of precision glass microspheres (d=0.0115-in.) were applied to the model surface near x/L= 0.1. The effects of the different forms of roughness will be detailed in a future report.

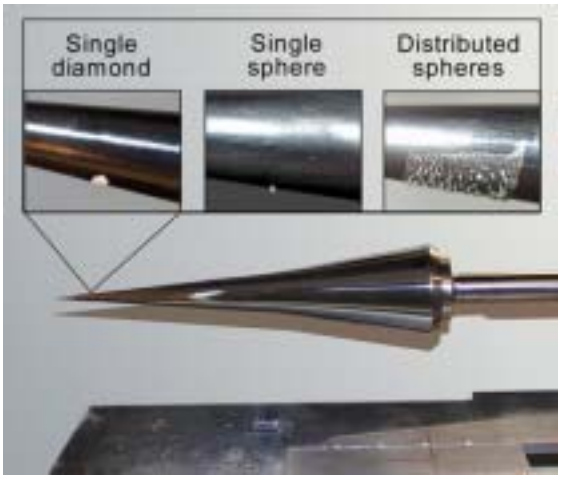

Fig. 2. 5 deg flared cone (Model 93-10) installed in the NASA LaRC 20-Inch Mach 6 Tunnel (boundary layer trips- inset).

Model Instrumentation

The original 5-degree straight cone was instrumented with a total of ninety-four type K (Chromel/Alumel) thermocouples that were tack welded to the model thin wall backside along a single ray. The thermocouples were spaced axially at 0.25-inch intervals. Access to the model interior was not possible and verification of the thermocouple locations was made by non-intrusive X-Ray measurements. The local model wall thickness was nominally 0.030-inch along the location of the streamwise row of thermocouples and 0.060-inch elsewhere (actual local wall thickness at each thermocouple junction was determined with ultrasound measurements-see Data Reduction and Uncertainty section). Forty-six 0.040-inch diameter static pressure orifices were located on the opposite side of the model although pressure measurements were not attempted with this model during the present test series.

The cone flare model was constructed and instrumentation locations determined in a similar fashion. A total of fifty-one type K thermocouples were tack welded to the model thin wall backside along a single ray. The thermocouples were spaced axially at 1-inch intervals between model stations x=2 and 9 inches and 0.25-inch intervals from model stations x=9 to 19.75-inches. The local model wall thickness was nominally 0.030-inch along the location of the streamwise row of thermocouples and 0.060-inch elsewhere. Twenty-nine 0.040-inch diameter static pressure orifices were located on the opposite side of the model.

Facility Descriptions

Although the Mach 6 NTC Quiet Tunnel has since been disassembled, at the time of the original quiet tunnel experiments, both facilities were located within the same lab and shared a common air supply line and heater element. For a short period, both were managed under what is now known as the Aerothermodynamic Laboratory Complex (ALC). This complex presently consists of four hypersonic wind tunnels that represent much of the nation's conventional aerothermodynamic test capability. Collectively, they provide a range of Mach number, unit Reynolds number, and normal shock density ratio[64]. This range of hypersonic simulation parameters is due, in part, to the use of two different test gases (air, and tetraflouromethane), thereby making the facilities unique national assets. The ALC facilities are relatively small and economical to operate, hence ideally suited for fast-paced aerodynamic performance and aeroheating, and transition studies aimed at screening, assessing, optimizing, and bench-marking (when combined with computational fluid dynamics) advanced aerospace vehicle concepts and basic fundamental flow physics research.

20-Inch Mach 6 Air Tunnel: Heated, dried, and filtered air is used as the test gas. Typical operating conditions for the tunnel are: stagnation pressures ranging from 30 to 500 psia; stagnation temperatures from 300 to 540 degree F; and freestream unit Reynolds numbers from 0.5 to 8 million per foot. A two-dimensional, contoured nozzle is used to provide nominal freestream Mach numbers from 5.8 to 6.1. The test section is 20.5 by 20 inches; the nozzle throat is 0.399 by 20.5-inch. A bottom-mounted model injection system can insert models from a sheltered position to the tunnel centerline in less than 0.5-sec. Run times of up to 15 minutes were achieved for the adiabatic wall temperature measurements. For the transient heat transfer tests, the model residence time in

the flow was limited to 20 seconds. A detailed description of this facility may be found in Ref. 64

In an attempt to attenuate noise from upstream piping/air control valves, the settling chamber was enlarged and recently retrofitted with a series of acoustically damping porous screen elements. This technology[7] was based upon quiet tunnel experience at LaRC and was designed to reduce pressure fluctuations in the settling chamber to approximately 0.005 % of the stagnation pressure.

Mass flow and total temperature fluctuations were measured in this facility[65] at reservoir conditions (P_o = 125 psia and T_o = 410 degree F.) very close to the reservoir conditions associated with the quiet tunnel low disturbance condition (P_o = 130 psia and T_o = 350 degree F.). In that work, a dual wire constant temperature anemometer was used to infer mass and total temperature fluctuations of 2.4% and 1.4%, respectively. Freestream spectra from this study at 125 psia began to roll off at approximately 10 kHz with little measurable fluctuations above the electronic noise floor out to the limits of the measurement near 160 kHz. As discussed in Ref. 65, the mass fluctuations were converted to pressure fluctuations and were quoted as 3.4%, which the authors claim was comparable to the results of Ref. 66 which reported 2.8% using a pitot probe. These quantitative measurements were made prior to the addition of the acoustically damping porous screen elements in the settling chamber and should be repeated.

Mach 6 Nozzle Test Chamber Quiet Tunnel: Heated and dried air was used as the test gas. Typical low disturbance operating conditions for the tunnel were: stagnation pressures ranging from 80 to 130 psia, stagnation temperatures up to 350 degree F, and a maximum freestream unit Reynolds numbers of 2.8 million per foot. A contoured axisymmetric slow expansion nozzle was used to provide a nominal freestream Mach number of approximately 5.9. The nozzle exit diameter was 7.49 inches with the flow exhausting into an open jet test section; the nozzle throat diameter was 1.0-inch. This facility had no model injection system thus transient based heat transfer measurements could not be obtained. Run time for the adiabatic wall temperature measurements varied between 30 and 60 minutes. Details concerning the facility, the size of the quiet flow envelope and measurements of the disturbance environment are discussed in Ref. 12.

Test Conditions and Setup

Reservoir and corresponding free stream flow conditions for the present tests in the LaRC 20-Inch Mach 6 Air Tunnel are presented in Table 1. The quiet tunnel test condition is represented at P_o = 130 psia and T_o = 350 degree F. The freestream properties were determined from the measured reservoir pressure and temperature and the measured pitot pressure at the test section. The standard procedure used to compute flow conditions for the ALC facilities uses the viscosity formulation given by Chapman-Cowling and is detailed in Ref. 67. However, for the present test the computed Reynolds number was based upon the less accurate Sutherland formulation for viscosity to maintain consistency with the method employed to compute flow conditions for tests made in the LaRC Mach 6 NTC Quiet Tunnel. Computed Reynolds numbers based upon Sutherland's formulation are generally 5% lower relative to that inferred from Chapman-Cowling.

In the present test, the ratio of model base area to tunnel cross sectional area for the cone flare model (93-10) was 0.042 and 0.036 for the straight cone. In both wind tunnel experiments a base mounted cylindrical sting supported the conical models. A limited number of runs were made with an uncalibrated hotwire positioned in the freestream just outside the model shock layer. The probe was attached to a holder that was mounted to the cylindrical sting. Model angle-of-attack (pitch) and sideslip (yaw) were referenced to the geometric centerline of the tunnel and were set to zero in the tunnel using a combination of accelerometer based angular measurements and a laser alignment system. It should be recognized that *geometric* pitch and yaw angles may not represent actual *flow* pitch and yaw angles if flow angularity is present. A photograph of the sting supported cone flare model is shown in Fig. 2. Details of the cone flare model installation in the NASA LaRC Mach 6 NTC Quiet Tunnel can be found in Ref. 16.

Test Techniques

Adiabatic wall temperature: In the original stability experiments conducted in the low disturbance tunnel, the individual thermocouple temperature measurements were monitored with time and used to determine when the model had obtained a state near thermal equilibrium. The resulting temperature distribution was used to identify transition onset. The test procedure for the quiet tunnel measurements involved preheating the model by exposing it to hypersonic conditions for 30 to 60 minutes to achieve thermal equilibrium. For the adiabatic wall temperature measurements in the conventional tunnel test, the test procedure was designed to approximate as closely as possible this technique. That is, the model was injected into the hypersonic stream and allowed to reach a state near thermal equilibrium. Higher mass flow rates with the present conventional tunnel tests limited total run times to approximately 12 to 15 minutes depending on the desired Reynolds number. Temperature time histories obtained during each run were monitored and indicated when thermal equilibrium was approached. Typical time rate of change of temperature near thermal equilibrium was on the order of 0.5 degree per minute. At the low Reynolds number laminar conditions ($Re_\infty \leq 1.1 \times 10^6$) this criteria could not be reached and required that the model be preheated prior the start of the run.

The model was not allowed to cool between runs in order to minimize the time required to reach thermal equilibrium on subsequent runs.

Transient thin skin heat transfer: The thin wall construction of the conical models made it possible to apply the transient thin skin calorimetery measurement technique to infer heat transfer distributions along the streamwise array of thermocouples. The lack of a model injection system and placement of the model inside the nozzle prevented this type of heating technique to be exploited in the low disturbance tunnel. In the current conventional tunnel test, separate tunnel runs were required to obtain transient heating data and adiabatic wall temperature data. For the transient technique, the hypersonic stream conditions were established with the model in a sheltered position. The model was then injected into the flow and thermocouple temperature time histories were acquired. The model was allowed to cool between runs in order to obtain isothermal conditions necessary for the calculation of heat transfer.

Surface static pressure: Surface pressure measurements were obtained concurrent with the adiabatic wall temperature or heat transfer data and were made with an electronically scanned pressure (ESP) transducer. The full-scale range of the absolute pressure transducer was 0.36 psia. The long run times associated with the adiabatic wall temperature measurements provided more than adequate time for settling. The relatively short test times associated with the transient heating measurements did not provide enough settling time. Although not presented in this report, the flared cone surface pressure distributions were utilized to determine if the model had any angle of attack issues such as those associated with the previous tests in the low disturbance tunnel[24].

Flow Visualization: Flow visualization in the form of schlieren was used to verify model incidence angle and to complement the surface temperature and heating measurements. The LaRC 20-Inch Mach 6 Air Tunnel is equipped with a pulsed white-light, Z-pattern, single-pass schlieren system with a field of view encompassing the entire test core. The model length did not permit an entire view of the cone flare length. The light source was pulsed for approximately a 3 ms duration. Images were recorded on a high-resolution digital camera and will be enhanced with commercial software for future analysis.

Data Reduction and Uncertainty

A 16-bit analog-to-digital facility acquisition system was used to acquire data. The facility, model thermocouple, and pressure data was collected by this system at a rate of 50 samples per second over a 20 second interval during each run. The raw data were transferred to a Hewlett-Packard 9000 computer for data reduction and storage.

Thermocouple mV output was referenced to an electronic ice point and was converted to engineering units via a standard type K lookup table. Accuracy of the surface temperature measurement is estimated to be better than ±5 degrees F. Heating rates under transient conditions were calculated from backside surface temperature measurements as discussed in detail in Ref. 68. The data were not corrected for surface conduction or curvature effects. The resulting heating distributions are presented in the form of a normalized heating coefficient, h/h_{ref} where h_{ref} corresponds to the theoretical stagnation point heating to a sphere using the method of Ref. 69. The reference radius is 0.125-inches which corresponded to the nosetip of largest bluntness. The conical models were originally designed to measure adiabatic wall temperatures and thus precise wall thickness measurements critical for inferring accurate heating magnitudes were never obtained. To improve the accuracy associated with the heating distributions obtained from the present tests, ultrasound measurements made at the vicinity of the thermocouple junction were used to determine the local wall thickness. Deviations from the nominal 0.030-inch wall thickness specified in the model drawings were noted and accounted for in the data reduction. For the transient thin skin heating measurements, the overall experimental uncertainty is estimated to be better than ±15%. Conduction effects near the model base may have contributed to a larger uncertainty in this region. Repeatability of the cone flare normalized heat transfer distribution over several wind tunnel entries with two sharp nosetips was found to be generally better than ±5% as shown in Fig. 3 and is representative of the entire test series. As the primary goal of the present test was the determination of transition onset, the accuracy of the heating measurements were more than adequate for indicating the departure from a reference laminar boundary layer state.

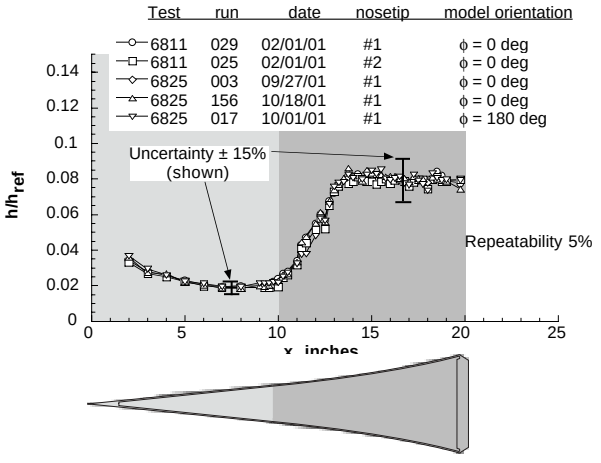

Fig. 3. Repeatability of heating distribution in conventional Mach 6 Tunnel. 5 deg. flared cone, M_∞=6 (conventional), Re_∞=4.3 x 10^6/ft, α=0 deg, R_n=0.0001-in.

The ESP pressure measurement system was calibrated prior to each run. The measured surface pressure was expressed in nondimensional form, P_s/P_∞, and in terms of a pressure coefficient. Measured reservoir values of P_O and T_O are estimated to be accurate to within ±2 percent.

The accurate determination of angle of attack was of utmost importance for the present slender cone tests as small model angles of attack relative to the flow can have a large effect on the theoretically computed frequency of the most unstable second-mode disturbance [26]. The angle of attack of the cone models was set to zero degrees by placing two calibrated accelerometer based inclinometers along the 0 and 180 degree rays of the cone surface. A model incidence of zero degrees was inferred when the absolute angular magnitude of both inclinometers was equal. Uncertainties in model angle-of-attack associated with accelerometer based measurements are estimated to be ±0.07 degree. As shown in Fig. 3, rolling the model 180 degrees produced no changes in the heating distribution and indicated that flow angularity was not an issue. Based on schlieren images, the model incidence was observed to change by no more than 0.05 degree due to thermal gradients in the support hardware during the long duration runs. The sideslip angle of the cone models was set to zero degrees by alignment of a laser light sheet along the longitudinal array of pressure orifices. Uncertainties in model sideslip angle associated with optical based measurements are estimated to be ±0.2 degree.

Computational Methods

Preface

Mean flow computations associated with the sharp nose conical models were performed with two Navier-Stokes solvers. LAURA, the benchmark code of the Aerothermodynamics branch at NASA LaRC, was used to provide straight cone surface heating predictions for comparison with laminar and turbulent measurement. Predictions provided by CFL3D were used to obtain boundary layer profile inputs used in the subsequent boundary layer stability analysis on the flared cone.

Mean Flow Calculations - LAURA

Computations were performed using the LAURA[70-71] code (version 4.9.2). The LAURA (Langley Aerothermodynamic Upwind Relaxation Algorithm) code is a three-dimensional, finite-volume solver which includes perfect-gas, equilibrium and non-equilibrium chemistry models, and can be used to solve the inviscid, thin-layer Navier-Stokes, or full Navier-Stoke equations. For the current study, the thin-layer Navier-Stokes equations were solved. Laminar computations were performed to determine heating rates for comparison with the laminar wind tunnel data, and to obtain boundary layer edge-parameters for future correlations. Turbulent computations were performed for comparison with turbulent wind tunnel data using the algebraic Baldwin-Lomax[72] model with modifications[73] for compressible flow and either a zero-length or Dhawan-Narashima[74] transition length model. The transition onset location for the computations was determined from the wind tunnel data. Solutions were computed on an axisymmetric, single-block (101 x 65) point grid. Grid adaptation was performed to align the bow-shock with the grid and produced nominal wall cell Reynolds numbers on the order of 10. Freestream conditions for the LAURA wind tunnel computations were set to the freestream operating conditions of the current test, which are listed in Table 1. For the wind tunnel computations, a uniform, ambient 80 degree F model wall temperature boundary condition was imposed.

Mean Flow Calculations - CFL3D

Mean flows around the cone used in the stability predictions were computed using CFL3D[75-76], which solves the compressible, three-dimensional, thin-layer Navier-Stokes equations with a finite-volume formulation. The code is characteristic-based, where upwind-biased spatial differencing is used for the inviscid terms. The flux-difference-splitting method of Roe[77] was used to obtain fluxes at the cell faces. All viscous terms were centrally differenced. The code provides for a variety of techniques that were used to accelerate convergence to steady state. In addition to local time-stepping, grid sequencing and multi-gridding were used. Grid sequencing allows the user to establish a converged or partially converged solution on a coarser grid before proceeding to a finer grid level. Multigridding is used to eliminate long-wavelength errors on the finer grids, and thereby improve convergence.

Except where indicated, the calculations were performed using adiabatic wall conditions on the cone surface. Extrapolation was used as the downstream (outflow) boundary condition and the free stream conditions specified in Table 1 were specified upstream of the cone and were used as the far-field condition. The shock was always captured within the domain.

The calculations were performed using a single-block grid with 137 nodes in the streamwise direction and 257 nodes in the cross-stream direction. The flow was forced to be axisymmetric by computing only a single azimuthal cell with width of 1 degree and periodic boundary conditions. Seven nodes of the streamwise grid are upstream of the nose of the cone; the eighth node coincides with the sharp cone tip. Four levels of multi gridding were applied at the finest grid. At least 50,000 iterations were used on the finest grid for each calculation. Additional iterations resulted in negligible changes to the computed flow.

At a unit Reynolds number of 6.2 x 10^6/ft (not shown), the results using the full grid were compared with the results using a grid consisting of every other point in the streamwise and cross-stream directions. A pointwise comparison of the computed velocities

indicated that less than 1% of the points had velocities that differed by more than 2% between the full and reduced grid. Almost all of the differences that exceeded 2% were confined to the most upstream points, where the flow is stable and would likely result in minimal influences on the stability calculations.

Because the flow upstream of the flare is that of a simple sharp cone, this portion of the flow was also computed using a boundary-layer code. Results of the stability analysis using profiles from the boundary-layer code and from CFL3D were indistinguishable and indicated that the boundary layer was properly resolved in the Navier-Stokes calculations. Stability calculations for different grid resolutions in the wall-normal direction also indicated that the 137 x 257 grid gives grid-converged stability results. Unlike the previous investigation by Balakumar and Malik[26] using an earlier version of CFL3D, a solution sensitivity to the flux limiters and level of convergence was not observed. In all cases, the default min-mod limiter was used.

Linear Stability Analysis

Stability analysis is performed using the Langley Stability and Transition Analysis Code (LASTRAC[78]. The LASTRAC code provides both quasi-parallel Linear Stability Theory (LST) and Parabolized Stability Equations (PSE) methods for stability analysis and N-factor correlation of boundary layers. The current release of LASTRAC can handle 2-D, axisymmetric or infinite swept-wing boundary layers. Three major computational modes; quasi-parallel LST, linear PSE, and nonlinear PSE can be chosen. Effects of streamwise curvature due to the flare and transverse curvature associated with the axisymmetric geometry are included in the stability analysis. Transverse curvature has a stabilizing influence on the axisymmetric first and second modes and a destabilizing influence on the asymmetric first mode disturbances[79]. Streamwise curvature is not important in the case of a flared cone since the dominant effect on the stability results is associated with the strong adverse pressure gradient. At a free-stream Mach number of 6, the boundary layer edge Mach number is approximately 5.4. Theoretically, the dominant instability mode on the flared cone is expected to be second mode. The second-mode wave is most unstable when it is two-dimensional or axisymmetric. All second-mode calculations presented here were done for axisymmetric waves. The asymmetric first-mode waves were computed by using different azimuthal wave numbers, n, defined as the number of waves along the azimuthal direction.

Results and Discussion

Preface

Discussion of the experimental results has been organized in the following manner. First, the results from the conventional hypersonic tunnel are presented and focus on the effects of Reynolds number, wall temperature ratio, nose bluntness, and angle of attack on transition onset. Bluntness and angle of attack trends are then compared to trends obtained from a *supersonic* quiet tunnel operated at low and high disturbance levels. The final section presents the direct comparison of transition onset between a conventional and low disturbance hypersonic wind tunnel using a common test model and transition detection method. To conclude, correlations of the transition onset location with linear stability prediction are made.

Conventional Tunnel

Transition Characteristics

Historically, many experimental methods[80-81] (surface and flowfield measurements) have been used to determine the location of boundary layer transition onset and the length of the transitional flow downstream that eventually leads to fully developed turbulent flow. In this study, surface heat transfer, a parameter of direct interest to designers of aerospace vehicles, was used to define transition onset. Normalized heat transfer distributions for the sharp tip (R_n=0.0001-inch) straight cone model are presented in Fig. 4a-c, for unit Reynolds numbers (Re_∞/ft) of 6.2 x 10^6, 4.3 x 10^6, and 1.1 x 10^6 respectively. For consistency, the onset of boundary layer transition at any given Reynolds number has been interpreted as the departure from the laminar heating distribution. For comparative purposes, laminar and two turbulent predictions are shown in each figure. Turbulence in the computations was initiated instantaneously (zero transition length) from (1) the nose and (2) from the measured transitional peak. For clarification purposes, distinct points on the measured heating distribution curve at Re_∞=6.2 x 10^6/ft in Fig. 4a have been identified with transition onset and the transitional peak.

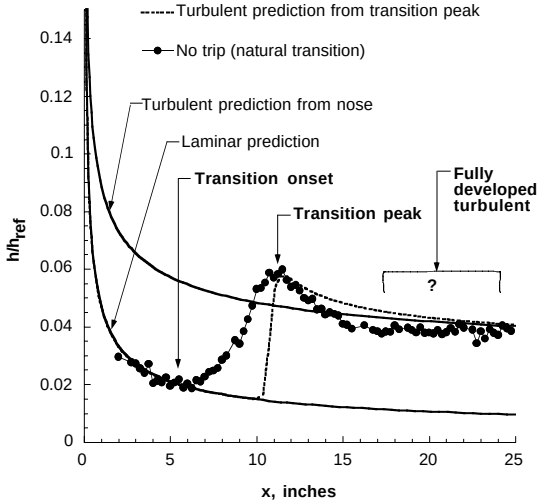

(a) Re_∞=6.2 x 10^6/ft

The transition peak has been shown to coincide with the point of maximum intermittency[82] and turbulent burst frequency[52]. At "high" Reynolds

number, the transition peak is clearly observed but typically becomes more difficult to identify as transition onset moves aft (e.g. lower Reynolds number or increased nose bluntness). The transition peak is often identified with the end of transition and hence the establishment of fully developed turbulent flow. Inspection of Fig. 4a suggests that the point of fully developed turbulent flow lies some distance downstream of the measured transitional peak and is consistent with the experimental observations of Refs. 52 and 82. This distinction, however, between the transition peak and fully developed turbulent flow is of importance when validating CFD turbulent heating prediction.

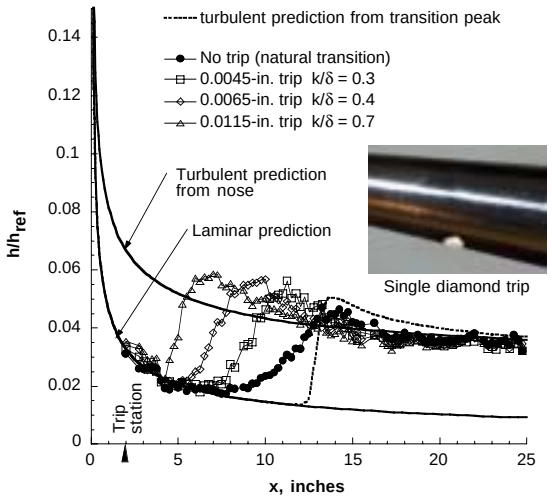

(b) Re_∞=4.3 x 10^6/ft

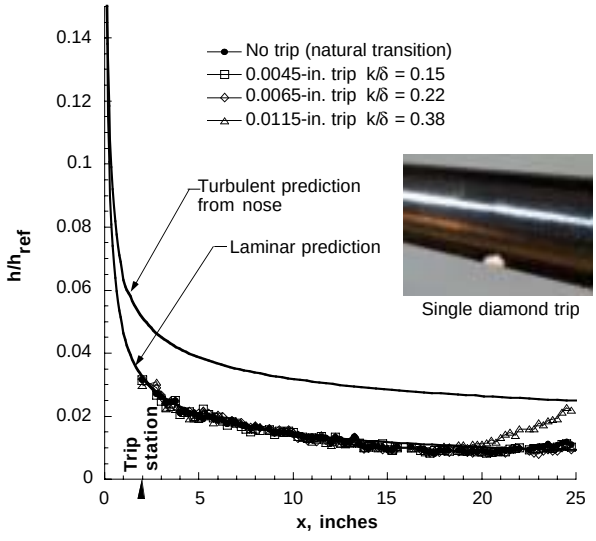

(c) Re_∞=1.1 x 10^6/ft

Fig. 4. Comparison of measured smooth and discrete trip heating distributions with laminar and turbulent prediction, 5 deg. straight cone, M_∞=6 (conventional), α=0 deg, R_n=0.0001-in.

In Fig. 4b, natural "smooth" body transition at Re_∞=4.3 x 10^6/ft has been compared to transition forced with discrete boundary layer trips. The ratio of trip-to-boundary layer height (k/δ) varied from 0.3 to 0.7. As expected, the larger trip heights are more effective at bringing transition onset closer to the trip location (x=2-in). Typical of all forms of roughness tested in the present study, agreement between the measured smooth wall and the forced turbulent heating with turbulent prediction was generally better than ±5%. In Fig. 4c natural "smooth" body transition at Re_∞=1.1 x 10^6/ft was not observed. The largest trip had only a marginal effect. Laminar heating predictions were generally within 5% of measurement.

Wall Temperature Ratio and Reynolds Number Effects

The heating distributions in Fig. 4 were inferred from temperature-time measurements whereby the model residence time in the flow was only a few seconds. The model wall temperature under adiabatic conditions (separate run-residence time in flow approximately 14 minutes) was, naturally, higher than that measured with the transient heating technique. Wall temperature can affect hypersonic transition. In the context of linear stability theory, hypersonic boundary layers on a slender cone near M_∞ = 6 would have both first and second mode disturbances. Wall cooling would be expected to stabilize first mode disturbances while destabilizing the second mode[83-84].

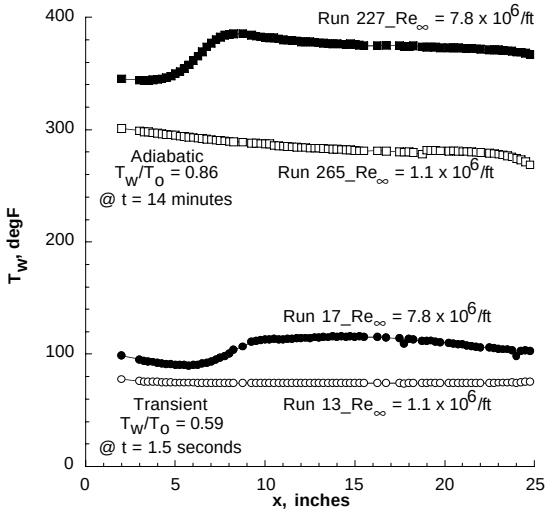

Fig. 5. Comparison of model temperature distributions for recovery temperature (adiabatic wall) and transient heating measurements, 5 deg. straight cone, M_∞=6 (conventional), Re_∞=1.1 and 7.8 x 10^6/ft, α=0 deg, R_n=0.0001-in.

A correlating parameter often used is the wall-to-total temperature ratio, T_w/T_o. The manner in which T_w/T_o is varied can impact the transition process in a ground based tunnel. Changing the stagnation temperature to produce a variation in T_w/T_o would likely

change the freestream disturbance environment[85]. In the present test series M_∞, Re_∞, and T_o were fixed and T_w was dictated by the model residence time in the flow. The difference in straight cone temperature is shown in Fig. 5, for the Reynolds number range in the conventional tunnel, Re_∞=1.1 x 10^6/ft and Re_∞=7.8 x 10^6/ft. The backside wall temperature distribution along the cone obtained 1.5 seconds after model exposure at the lowest Reynolds number was essentially constant (T_w=75 degree F; T_w/T_o=0.59). At the same Reynolds number under adiabatic conditions the wall temperature was higher (280 degree F; T_w/T_o=0.86). Similar wall-to-total temperature ratios were obtained at Re_∞=7.8 x 10^6/ft with surface temperature increases (385 degree F; T_w/T_o=0.90) associated with boundary layer transition near adiabatic conditions.

Despite the wall-to-total temperature differences in the present test on the sharp cone, the two methods for determining transition onset yielded equivalent locations for $Re_\infty < 3.2 \times 10^6$/ft as shown in Fig. 6a-d.

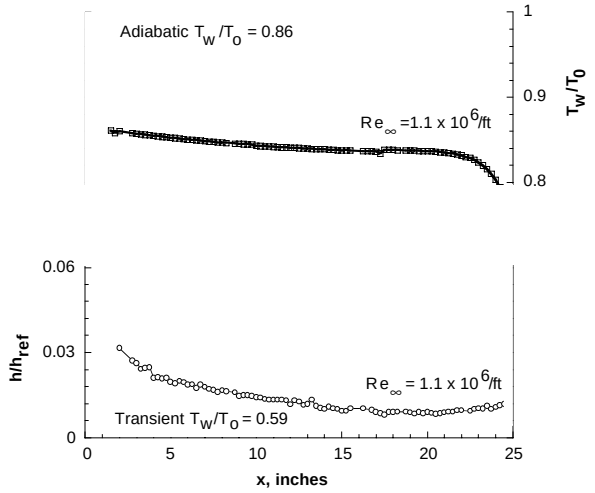

(a) Re_∞=1.1 x 10^6/ft, P_o = 60psi, T_o = 425 deg F

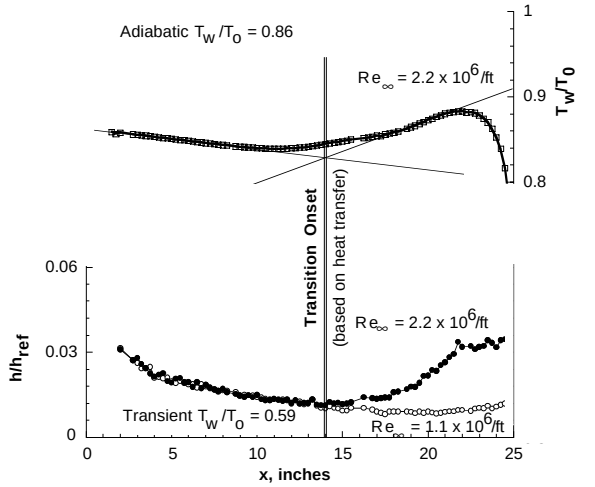

(b) Re_∞=2.2 x 10^6/ft, P_o = 125psi, T_o = 450 deg F

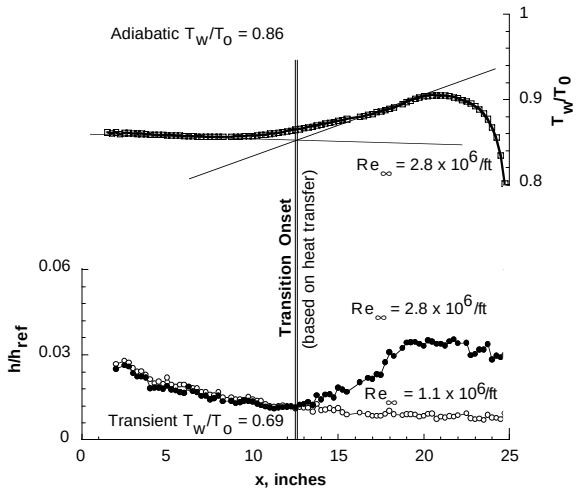

(c) Re_∞=2.8 x 10^6/ft, P_o = 130psi, T_o = 350 deg F

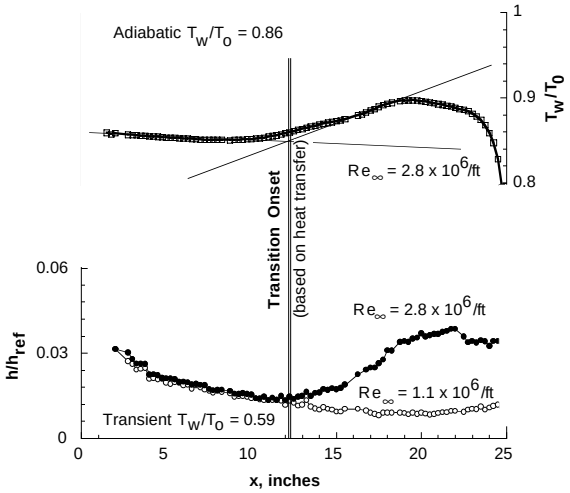

(d) Re_∞=2.8 x 10^6/ft, P_o = 155psi, T_o = 450 deg F

The transition onset point from the transient heating distributions (lower half of figure) has been indicated at a location where the nondimensionalized heating departed from laminar reference level measured at Re_∞=1.1 x 10^6/ft. The method for estimating transition onset via the adiabatic wall temperature distribution (upper half of figure) was consistent with that used for tests in the quiet tunnel and consisted of determining the intersection of two straight lines passing through the laminar region and the temperature rise near the transition peak as discussed in Ref. 16. While it is felt that the recovery temperature slope method is more subjective, the onset locations determined in this manner agree relatively well to those inferred via surface heating. Above Re_∞= 3.2 x 10^6/ft, Fig. 6e-h, small but consistent differences in the onset location became apparent. At Re_∞=6.2 x 10^6/ft, Fig. 6h, transition onset inferred from the heating distributions (T_w/T_o=0.59) was approximately 0.5-in.

downstream of that inferred from the adiabatic wall temperature distribution (T_w/T_o=0.86). This was not the anticipated trend whereby a decrease in T_w/T_o would be expected to destabilize the second mode resulting in a forward movement in the location of transition onset. It should be also noted that in several investigations conducted in conventional hypersonic facilities[51] little change in transition onset Reynolds numbers for .59<T_w/T_o< 0.86 were reported. Further discussion is deferred to the section devoted to correlation of measurement to linear stability prediction.

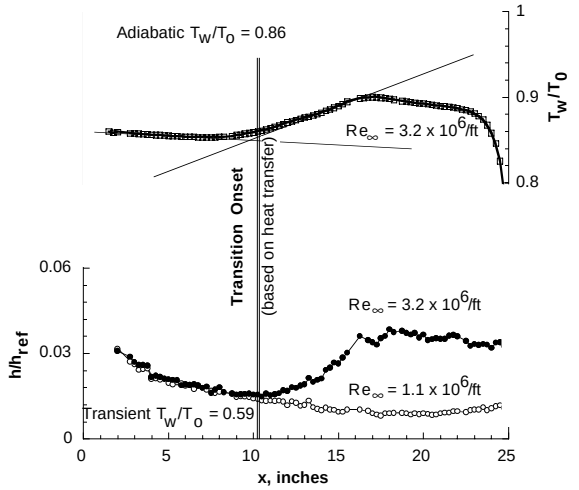

(e) Re_∞=3.2 x 10^6/ft, P_o = 180psi, T_o = 450 deg F

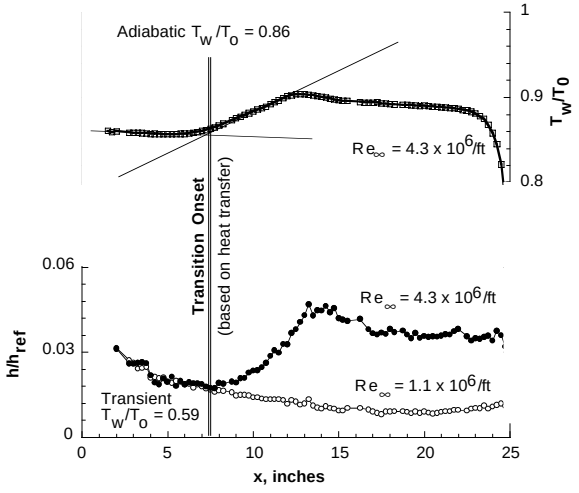

(f) Re_∞=4.3 x 10^6/ft, P_o = 250psi, T_o = 450 deg F

As expected, an increase in Reynolds number, Fig. 6a-h, moved the transition onset point on the cone surface upstream. The first indication of a transition peak (localized maximum in the nondimensionalized heating distribution) occurred at Re_∞ = 4.3 x 10^6/ft.

At Re_∞= 2.8 x 10^6/ft, the nominal reservoir temperature and pressure conditions corresponding to the quiet tunnel condition were 350 degree F and 130 psia, respectively. This relatively low temperature reservoir condition had been selected to reduce hot-wire overheat requirements for that test series. Concerns that this quiet tunnel operating condition lie too close to the air liquefaction curve were assessed in the conventional tunnel by testing at different reservoir pressure/temperature combinations so as to hold Re_∞/ft constant at Re_∞= 2.8 x 10^6/ft. The largest difference in transition onset, Fig. 6c-d, was approximately 0.25-in. and was considered insigificant.

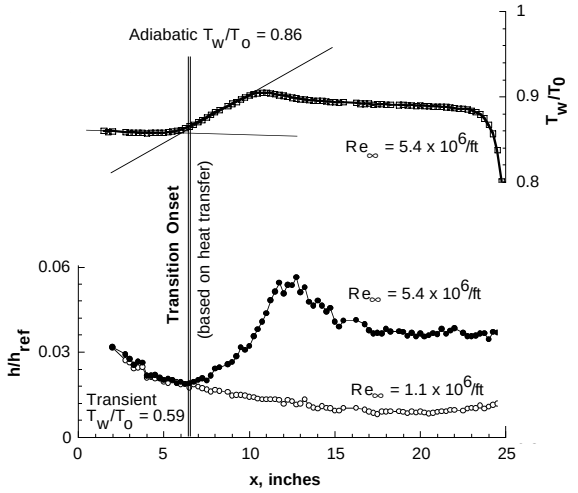

(g) Re_∞=5.4 x 10^6/ft, P_o = 325psi, T_o = 475 deg F

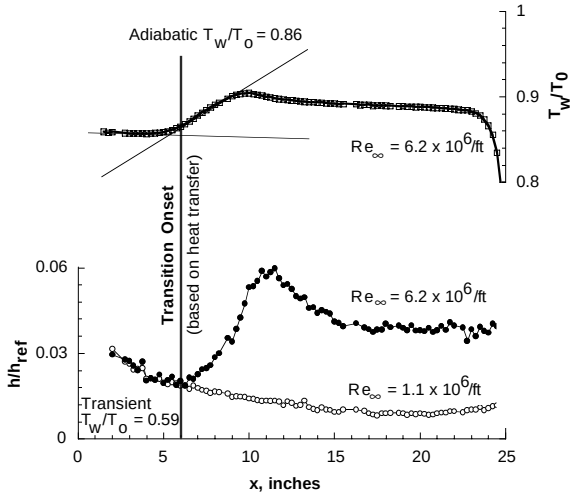

(h) Re_∞=6.2 x 10^6/ft, P_o = 365psi, T_o = 475 deg F

Fig. 6. Comparison of smooth body transition onset inferred from heating distributions with those determined via wall recovery temperature 5 deg. straight cone, M_∞=6 (conventional), α=0 deg, R_n=0.0001-in.

Bluntness Effects

While primarily intended to provide data for comparison to the quiet tunnel results, the present conventional tests also served to assess the effects of nose bluntness and angle of attack on transition onset.

The effect of nose bluntness at Re_∞= 7.8 x 10^6/ft is shown in Fig. 7a-c. Consistent with Ref. 50, nosetip bluntness delayed boundary layer transition. Transition onset for the sharp tip (R_n=0.0001-in.) occurred at x=5-inches with the transition zone extending at least another 10-in. downstream. An increase in the nosetip radius to 0.0625-inches extended the laminar boundary layer to x=12.25-inches with the transition zone extending perhaps to the end of the model.

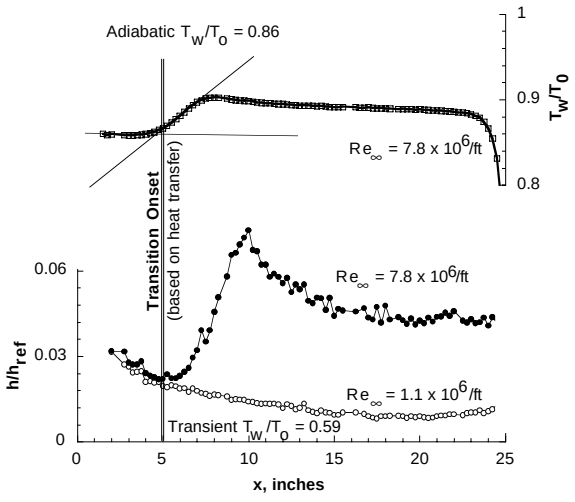

(a) R_n=0.0001-in.

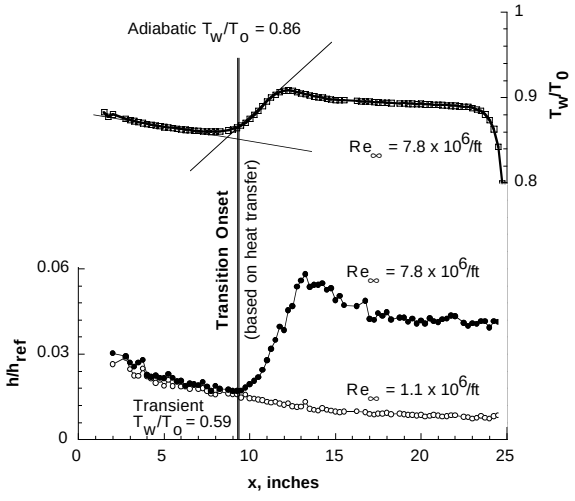

(b) R_n=0.03125-in.

The pronounced transition peak associated with the sharp nosetip, Fig. 7a, was attenuated as nose bluntness increased. For vehicle design, and in particular the hypersonic airbreather designed for sustained cruise, the observed heating overshoot associated with the transition peak may be of interest as the majority of slender hypersonic vehicles successfully flown have had some degree of bluntness (e.g. re-entry F). If thermal limitations associated with sharp leading edges are overcome (e.g. heat pipe technology, advanced ceramics) the so-called "transitional heating overshoot" could become more of a design factor in future TPS design.

At this Reynolds number, Re_∞= 7.8 x 10^6/ft Fig. 7a-c, the spatial disparity discussed in the previous section between transition onset locations obtained at T_w/T_o= 0.59 and 0.86 progressively increased to approximately 1-in. as the straight cone nosetip was blunted.

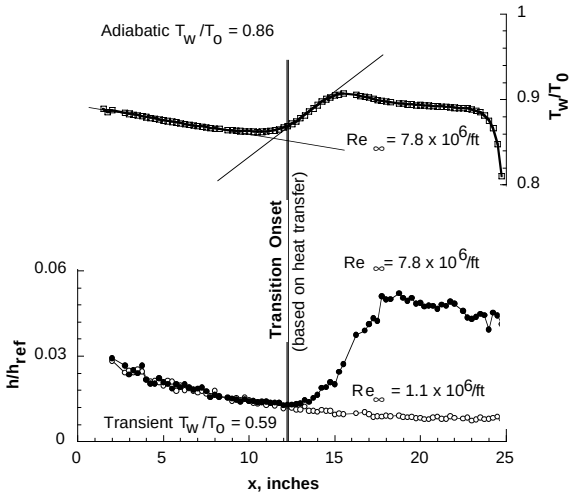

c) R_n=0.0625-in.

Fig. 7. Nose bluntness effects on smooth body transition onset inferred from heating and recovery temperature 5 deg. straight cone, M_∞=6 (conventional), α=0 deg, Re_∞=7.8 x 10^6/ft, P_0 = 475psi, T_0 = 475 deg F

Angle of Attack Effects

The effects of angle of attack on straight cone transition onset location are presented Fig. 8a-b, for three nosetip bluntnesses at Re_∞=7.8 x 10^6/ft and Re_∞=4.3 x 10^6/ft, respectively. For comparative purposes, the corresponding Reynolds number based upon freestream conditions and nose radius ($Re_{R,n}$) was also tabulated. The windward and leeward transition onset location has been normalized to the location measured on the sharp cone at α = 0 degree. Comparisons of the present data to other published data[47-49] obtained at similar test conditions with approximately the same model geometry are shown, Fig. 8a. The general trends appear consistent with these conventional tunnels. Specifically, for a *sharp* cone, an increase in angle of attack moved transition continuously rearward on the windward ray and forward on the leeward ray with no evidence of a reversal in transition onset location. Comparison of the data sets indicate that the laminar running length along the sharp cone windward ray in the LaRC conventional tunnel (relative to the corresponding sharp cone transition location at α = 0 deg) was greater than that inferred by Stetson and Krogmann (Refs. 47-49). As small

differences in θ_c and $Re_{R,n}$ exist between the data sets it is difficult to quantify the differences in magnitude.

The variation of the normalized transition location on the windward ray with angle of attack for the *blunted* cone exhibited a different trend than the *sharp* cone and are consistent with Stetson (Ref. 49).

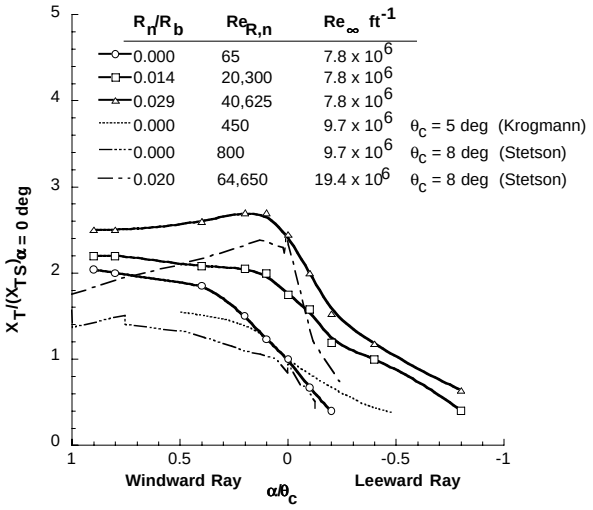

(a) Re_∞=7.8 x 10^6/ft, Krogmann M_∞=5. (Ref.47); Stetson M_∞=5.9 (Ref.49)

At the time, Stetson postulated that the effects of bluntness diminished with increasing angle of attack, thus the location of transition onset for the blunt nosetips would eventually cease to move rearward at some small incidence angle. In the present test, the location of transition onset for the bluntest nosetip (R_n = 0.125-in and $Re_{R,n}$ = 40,625), Fig. 8a, initially moved rearward for $\alpha/\theta_c < 0.2$ (hence the increased laminar running length with increasing incidence).

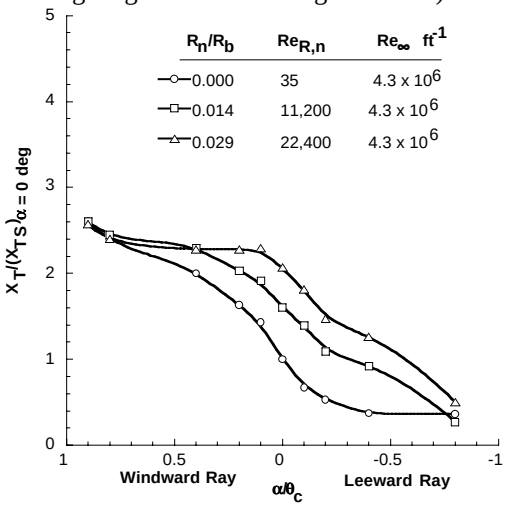

(b) Re_∞=4.3 x 10^6/ft

Fig. 8. Nose bluntness and angle of attack effects on windward/leeward-ray smooth body transition locations. Normalized to sharp cone values, 5 deg. straight cone, M_∞=6 (conventional)

In contrast to the sharp cone trend where transition continues to move rearward, the transition onset location for this bluntest nosetip reversed and began to move forward as incidence angle was further increased ($\alpha/\theta_c > 0.2$). At that time, Stetson conjectured that the blunt cone angle of attack trends (curves) would turn and eventually approach the sharp cone levels. The behavior postulated by Stetson was exhibited by the present data, Fig. 8b, for Re_∞=4.3 x 10^6/ft. Stetson's bluntness parameter was R_n/R_b and did not account for Reynolds number effects.

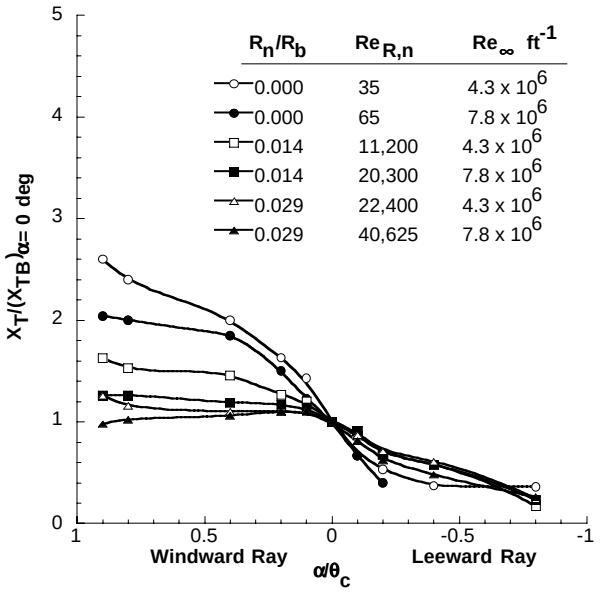

Fig. 9. Nose bluntness and angle of attack effects on windward/leeward-ray smooth body transition locations. Normalized to blunt cone values, 5 deg. straight cone, M_∞=6 (conventional)

In Fig. 9, the windward and leeward transition onset locations presented in Fig. 8a-b have been re-normalized to the location measured on the corresponding blunt nosetip at α = 0 degree. Expression of angle of attack trends in windward transition onset location in terms of the nose bluntness Reynolds number ($Re_{R,n}$) suggest that angle of attack effects ($\alpha/\theta_c < 1$) on transition onset appear to be mitigated for $Re_{R,n}$> 20,000.

Conventional Hypersonic and Low Disturbance Supersonic Comparisons

The effects of tunnel noise on high-speed laminar –turbulent transition are well documented and Schneider[5] presents an excellent review. When comparing hypersonic parametric trends inferred from measurements on a slender cone to those obtained at supersonic conditions, one must keep in mind that different instability mechanisms are most likely present. At supersonic conditions first mode instabilities prevail, while at the hypersonic conditions of the present tests,

both first and second mode instabilities are likely present.

Bluntness Effects

The effects of nose bluntness on slender cone transition in the presence and absence of a low disturbance freestream environment at supersonic conditions are presented in Fig. 10 (taken from Ref. 10).

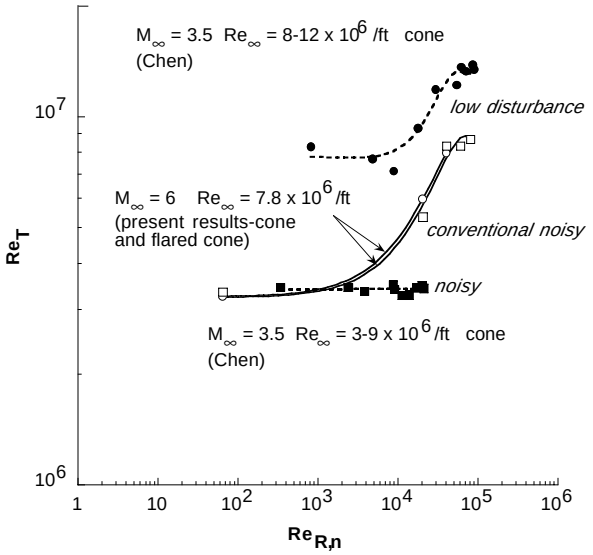

Fig. 10. Comparison of present nose bluntness effects on smooth body transition to supersonic trends (Ref.10) obtained in the NASA LaRC M=3.5 Quiet Tunnel at low and high disturbance levels. α=0 deg

The supersonic (M_∞ = 3.5) transition onset location was inferred from surface pitot pressure measurements made on a 5 degree half angle cone at α = 0 degree near adiabatic conditions. Chen's data presented in Fig. 10 were obtained in tabular form and limited to unit Reynolds numbers close to that obtained in the present test. The transition onset Reynolds number based on freestream conditions (Re_T) has been correlated against nose bluntness Reynolds number ($Re_{R,n}$) for both a low disturbance environment and at "noisy" conditions facilitated by closing the quiet tunnel boundary layer bleed slots. Chen and Schneider point out that under noisy conditions, small increases in nose bluntness did not delay transition in contrast to that inferred from tests under quiet conditions. The present M_∞=6 data were obtained in a conventional hypersonic tunnel at Re_∞=7.8 x 10^6/ft. This unit Reynolds number was selected so as to insure transition on the flared cone occurred upstream of the flare adverse pressure gradient (x = 10-in.) and transition onset measurements made on both the straight cone and the flared cone could be presented. Third-order polynomial fits to the data have been applied to clarify trends. Although the magnitude of Re_T at hypersonic conditions was different, it is clear that the conventional tunnel exhibits the same parametric trends as the supersonic data at low disturbance conditions (pronounced increase in Re_T with increasing nose bluntness Reynolds number). This suggests that perhaps the test section wall radiated noise from the quiet tunnel operating "noisy" is severe enough to mask the bluntness effect. In this special case, the parametric trend from the hypersonic conventional tunnel (at perhaps more moderate disturbance levels) appears to be qualitatively more consistent with that inferred from the supersonic tunnel operated at low disturbance conditions. At supersonic low disturbance conditions it appeared that bluntness effects initially became apparent for $Re_{R,n}$ between 10,000 and 20,000. Without additional measurements it is difficult to quantify the $Re_{R,n}$ threshold at M_∞ = 6 where bluntness effects prevail.

Angle of Attack Effects

The effects of angle of attack on slender cone transition in the presence and absence of a low disturbance freestream environment at supersonic conditions are presented in Fig. 11 taken from Ref. 9.

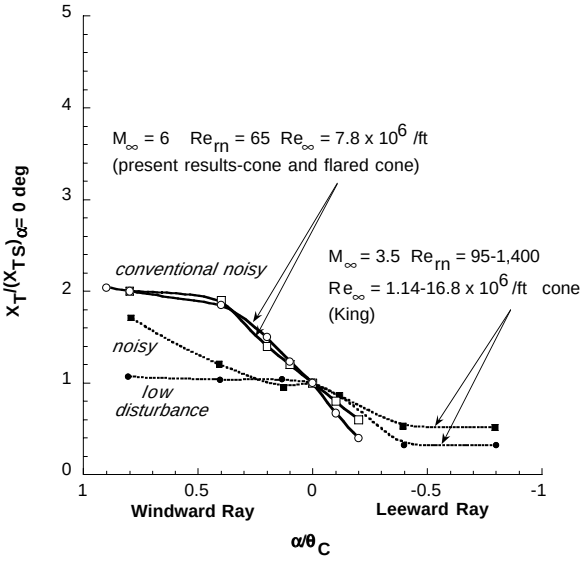

Fig. 11. Comparison of present angle of attack effects to supersonic windward/leeward-ray smooth body transition locations (Ref. 9) obtained in the NASA LaRC M=3.5 Quiet Tunnel at low and high disturbance levels. Normalized to sharp cone values

The supersonic (M_∞ = 3.5) transition onset location was inferred from surface pitot pressure measurements made on a 5 degree half angle cone at α = 0 degree near adiabatic conditions. The transition onset Reynolds number based on freestream conditions (Re_T) has been plotted against normalized angle of attack (α/θ_c) for both a low disturbance environment and at "noisy" conditions facilitated by closing of the quiet

tunnel boundary layer bleed slots. King observed that under supersonic low disturbance conditions, increases in angle of attack above $\alpha / \theta_c > 0.12$ did not produce a rearward movement of windward transition onset as was inferred from measurements under "noisy" conditions. The present M_∞=6 conventional hypersonic tunnel data were obtained at Re_∞=7.8 x 10^6/ft and did not exhibit this behavior. As in Fig. 10, this unit Reynolds number was selected so as to ensure transition on the flared cone occurred upstream of the flare adverse pressure gradient (x = 10-in.) and transition onset measurements made on both the straight cone and the flared cone could be presented. For these tests conducted at supersonic and hypersonic conditions, $Re_{R,n} < 1{,}500$. Curve fits to the data have been applied to clarify trends. It is clear that the conventional tunnel exhibited the same parametric trend as the supersonic data at "noisy" conditions. In this special case, the parametric trend from the conventional tunnel appears to be opposite to that inferred from the supersonic low disturbance tunnel. The trends displayed in the supersonic low disturbance facility remain inconclusive as the aft end of the cone was outside the region established as "quiet".

Comparison of Hypersonic Transition Onset in a Conventional and a Low Disturbance Facility

A direct comparison of conventional vs. low disturbance tunnel transition onset locations at adiabatic wall conditions for the straight and flared cone at comparable freestream conditions is shown, Fig. 12a-b, for Re_∞=2.8 x 10^6/ft. To the author's knowledge this represents the first comparison of transition onset location between a conventional and low disturbance hypersonic tunnel utilizing common models and transition detection techniques.

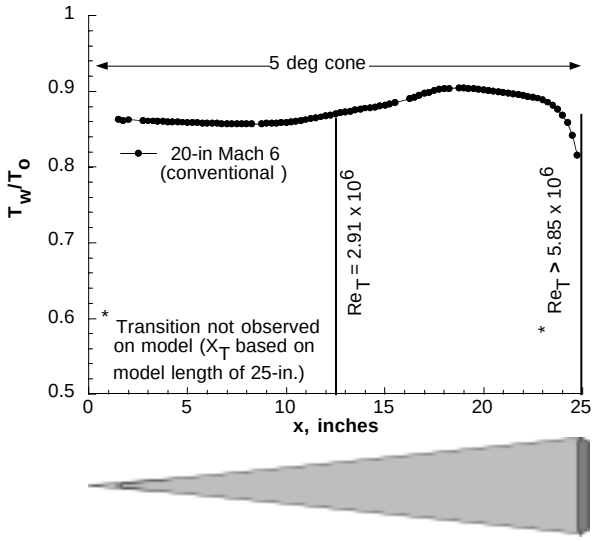

(a) 5 deg cone.

The conventional tunnel straight cone transition onset location (Fig. 12a) inferred from the wall temperature distribution near adiabatic conditions was located x = 12.5-in. at a corresponding transition Reynolds number (Re_T) of 2.91 x 10^6/ft. The method for estimating transition onset via the adiabatic wall temperature distribution was consistent with that used for tests in the quiet tunnel and consisted of determining the intersection of two straight lines passing through the laminar region and the sharp temperature rise near the transition peak (see Fig. 6d) as discussed in Ref. 16. At the corresponding unit Reynolds number in the Mach 6 Nozzle Test Chamber Quiet Tunnel, the boundary layer on this same model remained completely laminar[16]. Thus, based upon the 25-in. model length $Re_T \geq 5.85 \times 10^6$. The transition onset Reynolds number under low disturbance conditions is a factor of 2 or more relative to that measured on a straight cone in the LaRC conventional hypersonic tunnel. This is comparable to the factor of 2.3 measured on a straight cone by Ref. 9 at supersonic "quiet" and "noisy" conditions. Unfortunately, the hypersonic low disturbance tunnel was not operated "noisy" for the limited tests conducted with the straight cone model and a direct comparison to a conventional tunnel measurement cannot be made.

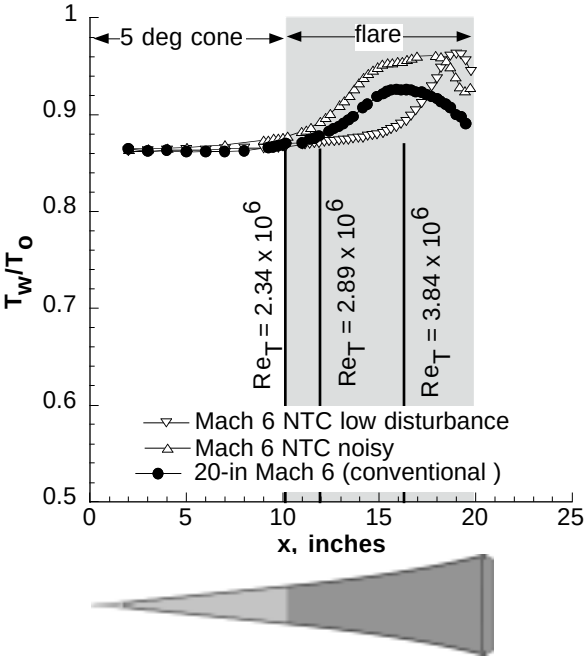

(b) 5 deg flared cone

Fig. 12. Comparison of present smooth body transition onset locations to that obtained in the NASA LaRC M=6 NTC Quiet Tunnel at low and high disturbance levels. M_∞=6, Re_∞=2.8 x 10^6/ft, α=0 deg, R_n=0.0001-in.

Because transition on the straight cone was not observed in tests conducted in the Mach 6 Nozzle Test Chamber Quiet Tunnel, emphasis of the stability tests was placed on the flared cone. The flare was designed to produce a nearly constant boundary layer thickness that was expected to enhance the likelihood of transition via

the second mode rather than the first mode. Since the most unstable second mode frequency is determined by the boundary layer thickness, the integrated N factor for the second mode becomes larger than that associated with the first mode. The geometry modification was successful and transition onset from second mode instability on the flared cone model in the low disturbance tunnel run "quiet" occurred at x = 16.25-in (Re_T = 3.84 x 10^6)[16] as indicated in Fig. 12b. The influence of acoustic disturbances on flare cone hypersonic transition was conservatively estimated by running the quiet tunnel in a "noisy" mode (diverter valves normally open to promote a laminar nozzle wall boundary layer are closed resulting in a turbulent nozzle boundary layer). As expected, transition onset moved forward to x = 10-in. (Re_T = 2.34 x 10^6).

In the "noisy" mode of the hypersonic low disturbance tunnel, transition onset occurred earlier than that measured in the conventional hypersonic tunnel, Fig. 12b, which suggests higher levels of freestream acoustic radiation relative to a conventional tunnel. The conventional tunnel flared cone transition onset location inferred from the wall temperature distribution near adiabatic conditions was located at x = 12.25-in. with a corresponding transition Reynolds number (Re_T) of 2.89 x 10^6. The transition onset Reynolds number under low disturbance conditions is a factor of 1.3 greater to that measured on flared cone in the LaRC conventional hypersonic tunnel and a factor of 1.6 relative to the flared cone run in the quiet tunnel run "noisy". It is noteworthy that transition onset between the straight cone and the flared cone occurred within a distance of 0.25-inch of each other and suggests that the initial boundary layer instability and growth primarily occurred in the zero pressure gradient region on the flared cone (x $\leq$ 10-in.).

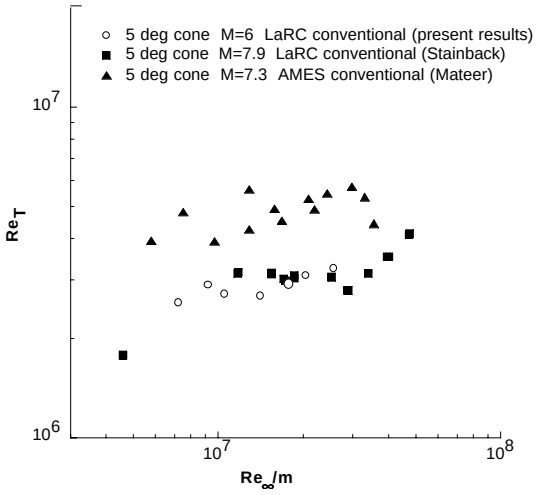

(a) Cones at hypersonic conditions as reported in (Refs. 53, 54)

Comparison of hypersonic unit Reynolds number effects on 5 degree sharp cone transition onset (taken from Refs. 53 and 54) with the present straight cone data are shown in Fig. 13a. The present data and that from Stainback are similar in magnitude and exhibit the, so-called, unit Reynolds number effect whereby radiated noise intensity from the tunnel wall boundary layer varies with Reynolds number and dominates the smooth body transition process. More often than not, unit Reynolds number effects are presented log/log and the trends are characterized with a straight line fit (see Fig13b). The discrete data in Fig. 13a however, indicates the complexity of the transition process and the influence of wall radiated noise from the test section walls. Near Re_∞/m = 1 x 10^7 the LaRC results from Stainback and the present study plateau before resuming the nearly linear increase in Re_T with Re_∞/m. The Ames transition onset data from Mateer were obtained with Helium gas injection in the nozzle boundary layer which presumably affected the levels of the test section wall radiated noise. Their measurements indicate a much smaller variation in transition Reynolds number with increasing unit Reynolds number.

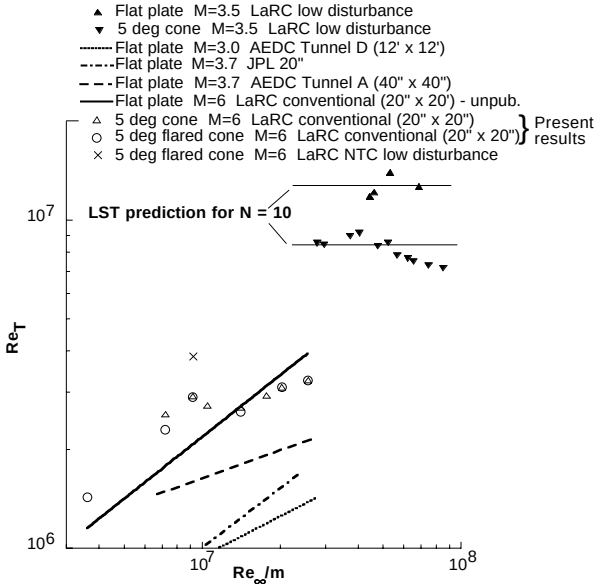

(b) Cones and flat plates at supersonic conditions as reported in (Ref.8)

Fig. 13. Comparison of transition onset Reynolds numbers with present data.

Reynolds number based on transition onset for cones and flat plates at supersonic conditions (taken from Ref. 8) with the present hypersonic straight cone and flared cone data are plotted against unit Reynolds number (per meter) in Fig. 13b. The AEDC results have been corrected to the onset of transition as indicated by Ref. 8. Also included is unpublished flat plate transition onset data also obtained in the conventional LaRC 20-Inch Mach 6 Air Tunnel. The present Mach 6 flared cone and flat plate data obtained in a conventional hypersonic tunnel exhibit the classic unit Reynolds number effect as discussed on the straight

cone in Fig. 13a. For $Re_\infty/m \geq 9 \times 10^6$ the straight cone and flared cone transition onset Reynolds numbers are very consistent despite the lower thermocouple spatial resolution on the flared cone model (and increased uncertainties in transition onset location) Above this value of Re_T, transition onset has occurred on the cone section of the flared cone and transition onset locations between the two models should be identical. As expected, below $Re_\infty/m = 9 \times 10^6$ a disparity between the transition onset Reynolds number for the two conical models developed due to the influence of the flare. At the lowest unit Reynolds number, the straight cone boundary layer was wholly laminar while the flare adverse pressure gradient has presumably destabilized the boundary layer and promoted transition on the model.

Linear stability theory at supersonic conditions suggest that transition should occur on cones at length Reynolds numbers that are lower than on flat plates. Measurements made in a low disturbance environment (namely the LaRC supersonic quiet tunnel[8]-not shown) are consistent with this prediction and have shown cone-to flat plate transition Reynolds number ratios less than unity-in the range of 0.8 to 0.9. In contrast, experimental data obtained in conventional tunnels have historically shown the opposite trend. Specifically, measurements at supersonic Mach numbers in conventional tunnels[80] have indicated cone-to flat plate transition Reynolds number ratios greater than unity-in the range of 2.2 to 2.5 (and 1.6 to 1.9 for $M_\infty = 6$). As suggested by Beckwith (Ref. 7) the observation that $Re_{T,cone} / Re_{T,plate} < 1$ (for conventional tunnels) may be due to the faster boundary layer growth on a flat plate relative to a cone and thus, stronger receptivity of the flat plate to the incident acoustic field from the turbulent test section walls found in the conventional tunnels.

Consistent with historical observations, the present data from the Mach 6 conventional tunnel ($Re_\infty/m \leq 1 \times 10^7$) indicate that the straight cone and flared cone transition onset Reynolds numbers were higher than the corresponding flat plate data (see Fig. 13b) and hence would yield cone-to flat plate transition Reynolds number ratios *greater* than one. However, for $Re_\infty/m \geq 1 \times 10^7$ the present data show that the straight cone and flared cone transition onset Reynolds number was actually lower than or nearly equal to that measured on the flat plate (see Fig. 13b) and hence would yield cone-to flat plate transition Reynolds number ratios *less* than one. Ironically, this observation at higher Reynolds numbers at hypersonic edge Mach numbers, is somewhat consistent with those made in the supersonic low disturbance tunnel. As noted in Ref. 5, the LaRC supersonic low disturbance tunnel run "noisy" also yielded cone-to flat plate transition Reynolds number ratios *less* than one (opposite to what was expected via Pate's[80] cone-to-flat plate transition findings) and was never fully explained.

In general, the flat plate transition onset Reynolds numbers from the conventional LaRC Mach 6 tunnel are consistently higher than the flat plate M=3 and 3.7 data from the AEDC and JPL facilities. Since it has been shown that the disturbance field sound intensity correlates with test section size[80] one might expect better agreement of the present smooth flat plate Re_T data to the JPL results. Despite the similar test section dimensions to the JPL tunnel, other factors such as Mach number effects on radiated tunnel wall noise, boundary layer receptivity on the flat plate, or the noise reduction technology in the conventional tunnel settling chamber may all have contributed to the higher Re_T values measured on the flat plate in the conventional LaRC 20-Inch Mach 6 Air Tunnel.

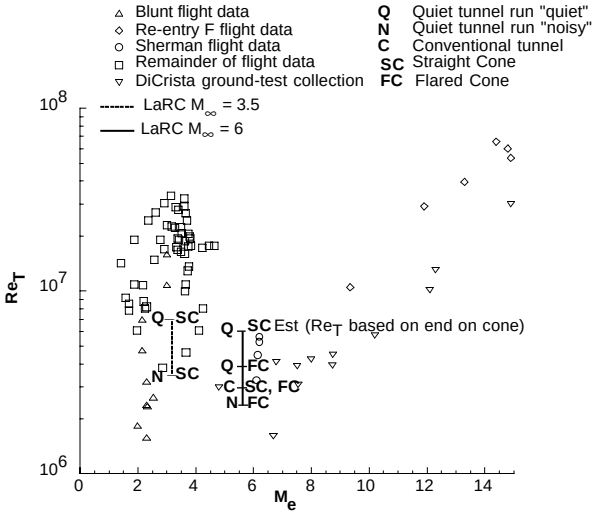

Fig. 14. Comparison of transition onset Reynolds number on sharp cones near zero angle of attack in flight and ground test as reported in (Ref. 86) with present data.

Figure. 14 (adapted from Fig. 1 of Ref. 86) shows both flight and ground based transition Reynolds numbers for a range of edge Mach number (see Ref. 86 for citations of these datasets). Variations of this figure are often used to indicate the inability of conventional ground facilities to properly simulate free flight conditions due to the higher disturbance levels generated from radiated noise from wind tunnel walls. It also shows an increase in transition onset Reynolds number with increasing Mach number suggested by flight and ground based measurements. The figure has been modified to include the present straight cone and flared cone results obtained at $M_e = 5.4$. Transition onset Reynolds numbers from the LaRC conventional hypersonic tunnel are generally consistent with the ground measurements reported by DiCrista (see Ref. 86) for sharp cones near $\alpha = 0$ degree and the flight results of Sherman (see Ref. 86).

Disturbance Environment and Correlation to Linear Stabilty Prediction

While the present conventional tunnel experimental data set has permitted direct comparison of transition onset to that measured in a hypersonic low disturbance tunnel, the lack of a one-to-one correspondence in terms of a stability experiment still exists. Characterization of the freestream disturbance environment and identification of dominate frequencies and associated growth rates are critical for any stability experiment conducted in a ground based facility. Exploratory tests to examine hot-wire survivability in the conventional LaRC 20-Inch Mach 6 Air Tunnel were conducted to determine the feasibility of obtaining future freestream and boundary layer spectra with a calibrated wire.

Preliminary free stream noise measurements were made with an uncalibrated hot-wire operated by a constant temperature anemometer. The addition of a two stage particulate filter appeared to have alleviated some of the concern with particulates (wire breakage) described in early hotwire measurements attempted in this facility[65]. Data (not shown) at reservoir pressures from 15 to 130 psi indicated that the free stream spectrum begins to roll off at approximately 10 kHz. At 15 and 30 psi the voltage spectra appear smooth with the exception of spikes clearly attributable to electronic noise. At reservoir conditions corresponding to conditions run in the low disturbance tunnel (P_o = 130 psi, T_o = 350 degree F) the spectrum contains spikes between 50 and 100 kHz, but it is impossible without more data to determine if they are flow or hot-wire related. At approximately 125 kHz the spectrum falls to the level of the instrument noise floor which is a factor of 250 below the spectral amplitude at 10 kHz. Qualitatively, it appeared that there were no *detectable* disturbances above the electronic noise level of the current instrumentation at the dominant second mode frequencies (see next section).

Mean flow and stability calculations were done at several unit Reynolds numbers listed in Table 1. In addition, the effects of wall temperature were examined by assuming a wall temperature of 80.3 degree F (300 K) to approximate the model surface temperature associated with the transient heating measurements. For all cases, the N factor, which represents how instability waves grow, was computed for a range of unstable disturbance frequencies. The predicted first-mode N factors as a function of the streamwise distance x for a unit Reynolds number of 2.89 x 10^6 /ft are shown in Fig. 15. The first-mode calculations were done at adiabatic wall conditions for a disturbance frequency ranging from 40 to 100 kHz and an azimuthal wave number from n = 3 to n = 30. The most amplified azimuthal wave number was found to be around 20 for most cases. The first-mode N factor at the measured transition onset location was approximately N = 2. The results shown in Fig. 15 were computed by integrating N factors for each individual asymmetric first mode wave. Alternatively, one can compute N factors by maximizing the growth rate (and thus, switch modes) at each downstream location. The latter method results in a larger N factor. Transition correlations for low speed infinite swept wing boundary layers indicate that tracking individual modes preserves more flow physics and yields better N factor correlation.

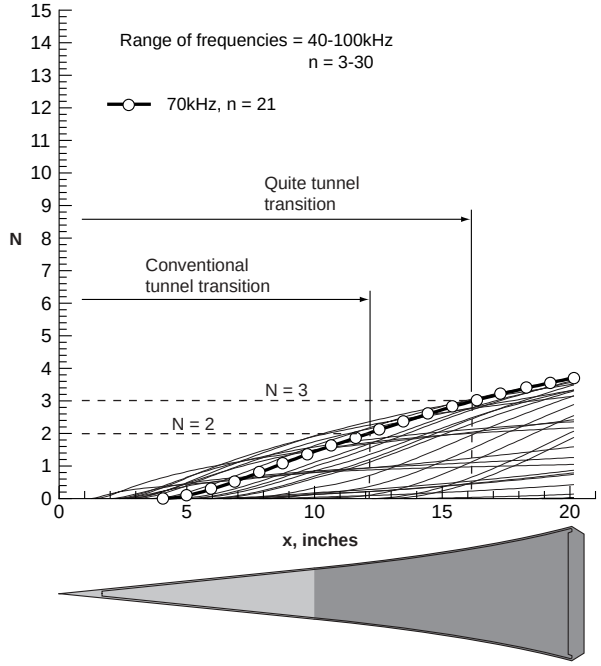

Fig. 15. Flared cone first-mode N factors of various disturbance frequencies and azimuthal wave numbers M_∞=6, Re_∞=2.8 x 10^6/ft, α=0 deg, R_n=0.0001-in., adiabatic wall condition

The corresponding second mode quasi-parallel LST N-factors of various disturbance frequencies (ranging from 20 to 340 kHz) are shown in Fig. 16a-b for cold wall and adiabatic wall conditions, respectively. The most unstable frequency under adiabatic conditions was predicted at 230kHz and is consistent with earlier flare cone stability predictions made by Balakumar[26]. The N-factor value at the measured transition onset location for this frequency was about 3.8 for the present investigation as compared to a value of about 7.8 under low disturbance conditions. The presence of both first and second mode disturbances on the conical models tested in the conventional tunnel is likely but cannot be verified at the present time as hot-wire measurements in the boundary layer were not attempted.

Several possible reasons have been suggested to explain the disparity in N-factor between the low disturbance and conventional wind tunnel environment. The differences in measured transition onset could be attributed to different transition mechanisms in the two experiments (e.g. first mode vs. second mode), as the N

factor for the most unstable first mode frequency was not much smaller than that predicted for the second mode (2 versus 3.8) but such an explanation is purely conjecture. A small N-factor at transition onset may also suggest that early nonlinear interaction could be present in the conventional wind tunnel due to a higher disturbance environment. An earlier investigation[87] using nonlinear PSE indicated that nonlinear effects were important for the Mach 8 sharp cone experiment conducted by Ref. 88. For the present experiment, nonlinear interactions involving both second-mode and asymmetric first-mode disturbances may contribute to transition. It is also possible that transition in the conventional tunnel may be the result of nonlinear mode interactions[28] and interpretation of the results based on linear stability theory may not be adequate. Further studies, both experimental and computational, are necessary to clarify these issues.

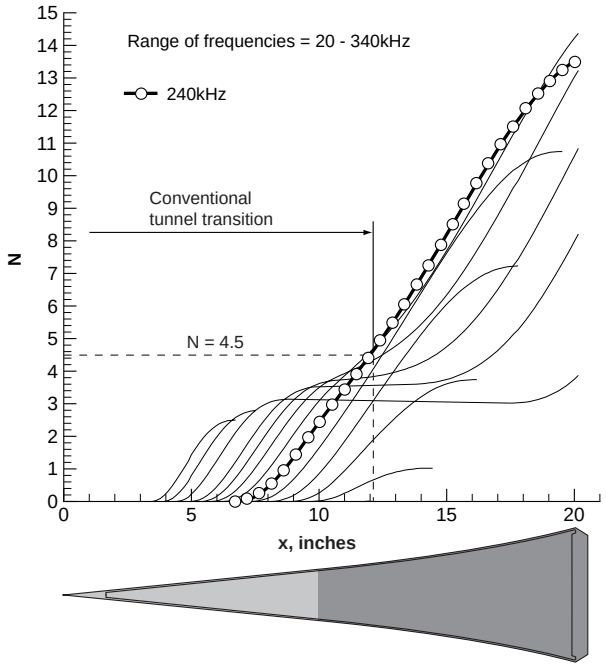

(a) Cold wall, T_w = 80.3 deg F (300K)

Instabilities associated with hypersonic boundary layers are quite sensitive to wall thermal conditions[83]. Stability calculations have indicated that wall-cooling destabilizes second-mode disturbances while stabilizing the first mode. Fig. 16a shows predicted flared cone second mode N factors obtained for a "cold" wall with a temperature of 80.3 degree F (300 K). As anticipated, the most amplified instability wave frequency increased to 240 kHz for the cold wall case because the boundary layer has thinned. This frequency is close to the earlier stability predictions by Balakumar[26] which indicated a slightly larger shift (up to 260kHz). Compared to the adiabatic wall case, the N factors increased by approximately 1.5 for the most amplified waves. Assuming the correlated N factor associated with second mode transition remained at 3.8, the predicted change in the transition onset location under cold wall conditions would be at most a 0.5-in. shift towards the nose. Experimentally, observations made on the sharp straight cone (see Fig. 6c) and on the sharp flared cone (not shown) indicated that the transition onset locations were indistinguishable for the adiabatic and transient cold-wall cases at Re_∞ = 2.8 x 10^6/ft. As the thermocouple spatial resolution was 0.25-in. the experimental results were not conclusive. The lack of movement in the transition onset location for adiabatic and cold wall conditions may also suggest that the linear amplification process is not as important in a conventional tunnel environment.

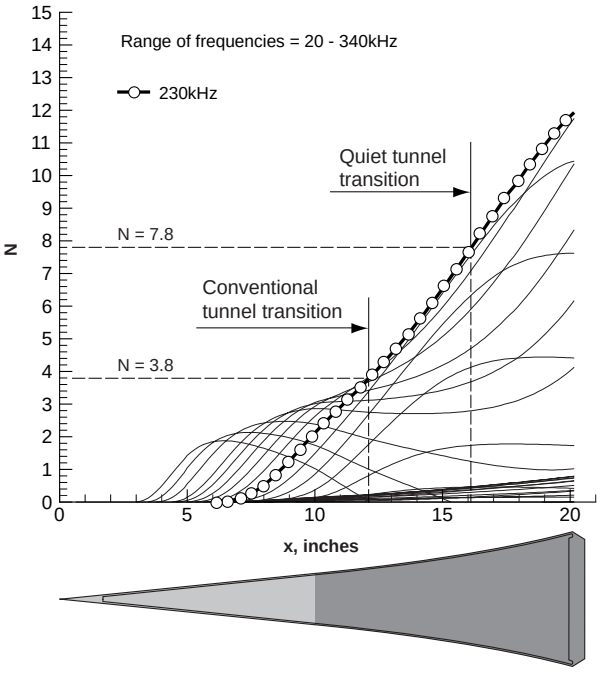

(b) Adiabatic wall condition

Fig.16. Flared cone second mode transition N-factor values for present Mach 6 transition onset location relative to that obtained in the NASA LaRC M=6 NTC Quiet Tunnel at a low disturbance level, M_∞=6, Re_∞=2.8 x 10^6/ft, α=0 deg, R_n=0.0001-in.

Table 2 summarizes the N values at transition onset for selected wind tunnel conditions. The table also includes second mode N factor values from linear PSE calculations. The PSE N factors are in general greater than the quasi-parallel LST N values, which are used more often in transition correlations. Greater N values in the linear PSE calculations may be attributed to non-parallel effects and the upstream shift of the neutrally stable location when PSE is employed. Similar effects have also been observed in earlier investigations[87,89] for hypersonic flat-plate and cone boundary layers. The N factors at transition onset for the present experimental measurements fall in a range of about 3 to 4.5 using linear stability theory and about 4 to 6.5 using linear PSE theory.

Concluding Remarks

Despite advances in supersonic/hypersonic quiet wind tunnel technology, relatively few low disturbance facilities exist. Those in existence today are typically deficient in Reynolds number relative to representative flight conditions, and are generally not operated in a manner conducive for fast-paced aeroheating assessment/screening studies. Thus, conventional hypersonic wind tunnels continue to serve as the primary source for experimental data from which to develop empirical methods for flight transition prediction.

The purpose of this paper was to qualitatively assess the acoustic disturbance environment of the NASA LaRC 20-Inch Mach 6 Air Tunnel and characterize facility noise effects on parametric trends associated with hypersonic slender body transition and to aid in the proper interpretation of transition criteria developed from data obtained in a conventional hypersonic tunnel. The relative disturbance environment of this conventional tunnel was expressed via differences in smooth wall transition onset locations measured on two conical models previously tested in the LaRC Mach 6 Nozzle Test Chamber (NTC) Quiet Tunnel. Together, the two sets of experiments are believed to represent the first direct comparison of transition onset between a conventional and low disturbance hypersonic wind tunnel using a common test model and transition detection method. The results of this study suggest that a low disturbance tunnel operated "noisy" is likely to produce higher levels of acoustic radiation relative to a conventional tunnel. In contrast to trends at supersonic conditions, bluntness effects on hypersonic transition were not attenuated by facility noise. At comparable freestream conditions, the transition onset Reynolds number under low disturbance conditions was a factor of 1.3 greater to that measured on flared cone in the LaRC conventional hypersonic tunnel and a factor of 1.6 relative to the flared cone in the low disturbance tunnel run "noisy". Navier-Stokes mean flow computations and linear stability analysis were conducted to assess the experimental results and have indicated N factors associated with transition onset to be a approximately a factor of 2 lower than that inferred from the corresponding low disturbance tunnel measurements. The lack of movement in the transition onset location for adiabatic and cold wall conditions may suggest that the linear amplification process is not as important in a conventional tunnel environment.

Acknowledgments

Without the assistance of the following individuals this work would not have been possible: Steve Wilkinson, Charlie Greenhalgh, Ed Covington, Pete Veneris, Ron Deans, and Kevin Meidinger for model design information, surface inspection support, and model refurbishment; John Ellis, Grace Gleason, Rowland Hatten, and Steve Jones for wind tunnel support; Sheila Wright and Mike Difulvio for data acquisition assistance; Steve Wilkinson, Steve Schneider, Rudy King, Feng-J. Chen, and Ndaona Chokani for analysis/computational support; Cathy McGinley for hot-wire measurements; and Richard Wheless for documentation assistance. The authors gratefully acknowledge their contributions and behind-the- scenes work.

References

1.Wuester, K. E., "An Assessment of the Impact of Transition on Advanced Winged Entry Vehicle Thermal Protection System Mass," AIAA Paper 81-0019, June, 1981.

2.Tartabini, P. V., "A Multidisciplinary Performance Analysis of a Lifting-Body Single-Stage-to-Orbit Vehicle," AIAA Paper 2000-1045, Jan., 2001.

3.Reed, H. L., Kimmel, R., Schneidner, S., and Arnal, D.,"Drag Prediction and Transition in Hypersonic Flow," AGARD-CP-600, Vol. 3, Dec., 1997.

4.Heiser, W. H., Pratt, D. T., *Hypersonic Airbreathing Propulsion*, edited by J. S. Przemieniecki,, AIAA Educational Series, AIAA, Washington, DC, 1994, pp. 41-45.

5.Schneider, S. P., "Effects of High-Speed Tunnel Noise on Laminar-Turbulent Transition," *Journal of Spacecraft and Rockets*, Vol. 38, No. 3, 2001, pp. 323-333.

6.Beckwith, I. E., and Miller, C. G., "Aerothermodynamics and Transition in High Speed Wind Tunnels at NASA LaRC," Annual Reviews of Fluid Mechanics, Vol. 22, 1990.

7.Beckwith, I. E., Chen, F. J., and Malik, M. R., "Transition Research in the Mach 3.5 Low-Disturbance Wind Tunnel and Comparisons of Data with Theory," SAE 892379, Sept., 1989.

8.Chen, F. -J., Malik, M. R., and Beckwith, I. E., "Boundary-Layer Transition on a Cone and Flat Plate at Mach 3.5," *AIAA Journal*, Vol. 27, No. 6, June, 1989, pp .687-693.

9.King, R. A., "Three-Dimensional Boundary-Layer Transition on a Cone at Mach 3.5," *Experiments in Fluids*, Vol. 13, 1992, pp. 305-314.

10.Chen, F.-J., "Boundary-Layer Transition Extent Measurements on a Cone and Flat Plate at Mach 3.5," AIAA Paper 93-0342, Jan., 1993.

11.Wilkinson, S. P., "A Review of Hypersonic Boundary-Layer Stability Experiments in a Mach 6 Wind Tunnel," AIAA Paper 97-1819, June., 1997.

12.Blanchard A. E., Lachowicz J. T., and Wilkinson S. P., "NASA Langley Mach 6 Quiet Wind Tunnel Performance," *AIAA Journal*, Vol. 35, No. 1, January, 1997, pp 23-28.

13.Blanchard A. E., Lachowicz J. T., and Wilkinson S. P., "Performance of the NASA-Langley Mach 6 Quiet Wind Tunnel," AIAA Paper 96-0441, January, 1995.

14.Lachowicz J. T., Chokani N., and Wilkinson S. P., "Boundary-Layer Stability Measurements in a Hypersonic Quiet Tunnel," *AIAA Journal*, Vol. 34, No. 12, Dec., 1996, pp 2496-2500.

15.Lachowicz J. T., Chokani N., and Wilkinson S. P., "Hypersonic Boundary Layer Stability over a Flared Cone in a Quiet Tunnel," AIAA Paper 96-0782. Jan., 1996.

16.Lachowicz J. T., "Hypersonic Boundary-Layer Stability Experiments in a Quiet Wind Tunnel with Bluntness Effects," Ph.D. Dissertation, Mechanical and Aerospace Engineering Dept., North Carolina State University, Raleigh, NC, November 1995.

17.Lachowicz J. T. and Chokani N., "Hypersonic Boundary Layer Stability Experiments in a Quiet Wind Tunnel with Bluntness Effects, NASA CR-198272, January, 1996.

18.Doggett, G. P., Chokani N., and Wilkinson S. P., "Effect of Angel of Attack on Hypersonic Boundary-Layer Stability," *AIAA Journal*, Vol. 35, No. 3, March, 1997, pp.464-470.

19.Doggett G. P., Chokani N., and Wilkinson S. P., "Hypersonic Boundary-Layer Stability Experiments on a Flared-Cone Model at Angle of Attack in a Quiet Wind Tunnel," AIAA Paper 97-0557, January, 1997.

20.Doggett G. P., "Hypersonic Boundary-Layer Stability on a Flared-Cone Model at Angle of Attack," Ph.D. Dissertation, Mechanical and Aerospace Engineering Dept., North Carolina State University, Raleigh, NC, May 1996.

21.Doggett G. P., and Chokani N., "Hypersonic Boundary-Layer Stability Experiments on a Flared-Cone Model at Angle of Attack in a Quiet Wind Tunnel," NASA CR 201617, October 1996.

22.Blanchard A. E., "An Investigation of Wall-Cooling Effects on Hypersonic Boundary-Layer Stability in a Quiet Wind Tunnel," Ph.D. Dissertation, Old Dominion University, Dept. of Mechanical Engineering, Norfolk, VA, December, 1995.

23.Blanchard, A .E., and Selby, G. V., "An Experimental Investigation of Wall- Cooling Effects on Hypersonic Boundary-Layer Stability in a Quiet Wind Tunnel," NASA CR-198287, February, 1996.

24.Chokani, N., "Perspective: Stability Experiments at Hypersonic Speeds in a Quiet Wind tunnel," AIAA Paper 2001-0211, Jan., 2001.

25.Malik, M. R., Balakumar, P., and Chang C.-L., "Effect of Adverse Pressure Gradient on the Second Mode Instability in Hypersonic Boundary Layers," High Technology Corporation,, Report No. HTC-9006, Dec, 1990.

26.Balakumar, P., and Malik M. R., "Effect of Adverse Pressure Gradient and Wall Cooling on Instability of Hypersonic Boundary Layers," High Technology Corporation,, Report No. HTC-9404, March, 1994.

27.Schneider, S. P., "Hypersonic Laminar Instability on Round cones Near Zero Angle of Attack," AIAA Paper 2001-0206, Jan., 2001.

28.McDaniel, R. D., and Hassan, H. A., "Role of Bypass Transition in conventional Hypersonic Facilities," AIAA Paper 2001-0209, Jan., 2001.

29.Mack L. M., "Linear Stability Theory and the Problem of Supersonic Boundary-Layer Transition," *AIAA Journal*, Vol. 13, No. 3, March, 1975, pp278-289.

30.Arnal, D., "Boundary Layer Transition: Predictions Based on Linear Theory," AGARD R-793, April, 1994.

31.Maslov, et. al., "Hypersonic Flow Stability Experiments," AIAA Paper 2002-0153, Jan., 2002.

32.Stetson, K. F., and Kimmel, R. L., "On Hypersonic Boundary-Layer Stability," AIAA Paper 92-0737, Jan., 1992.

33.Berry, S. A., Bouslog, S. A., Brauckmann, G. J., and Caram, J. M., "Shuttle Orbiter Experimental Boundary-Layer Transition Results with Isolated Roughness," *Journal of Spacecraft and Rockets*, Vol. 35, No. 3, 1998, pp. 241-248.

34.Berry, S. A., "Recent Shuttle Transition Results in the LaRC 20-Inch Mach 6 Tunnel," AIAA Paper 2002-2744, June, 2002.

35.Berry, S. A., Horvath, T. J., Hollis, B. R., Thompson. R. A., and Hamilton, H. H., "X-33 Hypersonic Boundary Layer Transition," *Journal of Spacecraft and Rockets*, Vol. 38, No. 5, 2001, pp. 646-657.

36.Thompson, R, A., Hamilton, H.H. II, Berry, S. A., and Horvath, T. J., "Hypersonic Boundary Layer Transition for X-33 Phase II Vehicle," AIAA Paper 98-0867, Jan., 1998.

37.Thompson, R. A., "Review of X-33 Hypersonic Aerodynamic and Aerothermodynamic Development," ICA 0323, August 2000.

38.Berry, S. A., Horvath, T. J., DiFulvio, M., Glass, C., and Merski, N. R., "X-34 Experimental Aeroheating at Mach 6 and 10," *Journal of Spacecraft and Rockets*, Vol. 36, No. 2, 1998, pp. 171-178.

39.Horvath, T. J., Berry, S. A., Merski, N. R., and Fitzgerald, S. M., "X-38 Experimental Aerothermodynamics," AIAA Paper 2000-2685, June, 2000.

40.Berry, S. A., Horvath, T. J., Roback, V. E., and Williams, G. B., "Results of Aerothermodynamic and Boundary Layer Transition Testing of 0.0362-Scale X-38 (Rev 3.1) Vehicle in NASA Langley 20-Inch Mach 6 Tunnel," NASA TM 112857, Sept., 1997.

41.Berry, S. A., Auslander, A. H., Dilley, A. D., and Calleja, J. F., "Hypersonic Boundary-Layer Trip Development for Hyper-X," *Journal of Spacecraft and Rockets*, Vol. 38, No. 6, 2001, pp. 853-864.

42.Nance, R. P., Hollis, B. R., Horvath, T. J., Alter, S. J., and Hassan, H. A., "Computational Study of

Hypersonic Transitional Wake Flow," *Journal of Thermophysics and Heat Transfer*, Vol. 13, No. 2, April-June 1999.

43.Horvath, T. J., Cheatwood, F. M., Wilmoth, R. G., and Alter, S. J., "Wake Closure Characteristics and Afterbody Heating On a Mars Sample Return Orbiter," *Innovative Transportation Systems for Exploration of the Solar System and Beyond*. STAIF /AIP Conference proceedings, Vol. 608, Feb., 2002, pp.318-336.

44.Horvath, T. J., McGinley, C. B., and Hannemann, K., "Blunt Body Near Wake Flow Field at Mach 6," AIAA Paper 96-1935, June, 1996.

45.Cheatwood, F. M., Merski, N. R., Riley, C. J., and Mitcheltree, R. A., "Aerothermodynamic Environment Definition for the Genesis Sample Return Capsule," AIAA Paper 2001-2889, June, 2001.

46.Hollis, B, R., and Liechty, D.S., "Boundary Layer Transition Correlations and Aeroheating Predictions for Mars Smart Lander," AIAA Paper 2002-2745, June, 2002.

47.Krogmann, P., "An Experimental Study of boundary-Layer Transition on a Slender Cone at Mach 5," AGARD-CP-224, May, 1977.

48.Stetson, K. F., and Rushton, G. H., "Shock tunnel Investigation of Boundary-Layer Transition at M = 5.5," *AIAA Journal*, Vol. 5, No. 5, May, 1967, pp. 899-906.

49.Stetson, K. F., "Mach 6 Experiments of Transition on a Cone at Angle of Attack," *Journal of Spacecraft*, Vol. 19, No. 5, Oct., 1982, pp. 397-403.

50.Stetson, K. F., "Comments on Hypersonic Boundary-Layer Transition," WRDC-TR-90-3057, Sept., 1990.

51.Maddalon, D. V., "Effect of Varying Wall Temperature and Total Temperature on Transition Reynolds Number at Mach 6.8," *AIAA Journal*, Vol. 7, No. 12, Dec, 1969, pp.2355-2357.

52.Owen, F., "Transition and Turbulence Measurements in Hypersonic Flows," AIAA Paper 90-5231, Oct., 1990.

53.Owen, F. K., Horstman, C. C., Stainback, P. C., and Wagner, R. D., "Comparison of Wind Tunnel Transition and Freestream Disturbance Measurements," *AIAA Journal*, Vol. 13, No. 3, Mar., 1975, pp.266-269.

54.Mateer, G. G., and Larson, H. K., "Unusual Boundary-Layer Transition Results on Cones in Hypersonic Flow," *AIAA Journal*, Vol. 7, No. 4, April, 1969, pp.661-664.

55.Zakkay, V., and Bos, A., "Laminar, Transitional, and Turbulent Flow with Adverse Pressure Gradient on a Cone-Flare at Mach 10," *AIAA Journal*, Vol. 5, No. 2, Feb, 1967, pp.201-207.

56.Kimmel, R. L., "The Effect of Pressure Gradients on Transition Zone Length in Hypersonic Boundary Layers," Journal of Fluids Engineering, Vol. 119, March, 1997.

57.Reda, D. C., "Review and Synthesis of Roughness-Dominated Transition Correlations for Reentry Applications," *Journal of Spacecraft and Rockets*, Vol. 39, No. 2, Mar.-Apr., 2002, pp. 161-167.

58.Bouslog, S. A., An, M. Y., and Derry, S. M., "Orbiter Windward-Surface Boundary-layer Transition Flight Data," NASA CP 3248 Part 2, April, 1995.

59.Bouslog. S. A., Moore, B., Lawson, I., and Sawyer, J. W., "X-33 Metallic TPS Tests in NASA-LaRC High Temperature Tunnel," AIAA Paper 99-1045, Jan. 1999.

60.Palmer, G., Kontinos, D., and Sherman, B., "Surface Heating Effects of X-33 Vehicle TPS Panel Bowing, Steps, and Gaps," AIAA Paper 98-0865, Jan. 1998.

61.Poll, D. I., "Laminar-Turbulent Transition," AGARD Advisory Report 319, Vol.1, 1996.

62.Takeshi, I., Randall, L. A., and Schneider, S. P., "Effect of Freestream Noise on Roughness-Induced Boundary-Layer Transition for a Scramjet Inlet," AIAA Paper 2000-0284, Jan, 2000.

63.Dietz, A. J., "Boundary-Layer Receptivity to Transient Convected Disturbances" *AIAA Journal*, Vol. 36,No. 7, July, 1998.

64.Miller, C. G., "Langley Hypersonic Aerodynamic/Aerothermodynamic Testing Capabilities - Present and Future," AIAA Paper 90-1376, June 1990.

65.Stainback, P. C., and Kubendran, L. R., "The Measurement of Disturbance Levels in the Langley Research Center 20-Inch Mach 6 Tunnel," NASA CR 4571, NAS1-19320, 1994.

66.Harvy, W. D., Stainback, P. C., and Srokawski, A. J., "Effect of Slot Width on Transition and Noise Attenuation of a Sound Shield Panel for Supersonic Wind Tunnels," AIAA 9th Aerodynamic Testing Conference Proceedings, June, 1976, pp. 198-222.

67.Hollis, B. R., "Real-Gas Flow Properties for NASA Langley Research Center Aerothermodynamic Facilities Complex Wind Tunnels," NASA CR 4755, Sept., 1996.

68.Miller, Charles G. III, "Comparison of Thin-Film Resistance Heat-Transfer Gages With Thin-Skin Transient Calorimeter Gages in Conventional Hypersonic Wind Tunnels," NASA TM 83197, Dec., 1981.

69.Fay, J. A., and Riddell, F. R., "Theory of Stagnation Point Heat Transfer in Dissociated Air," *Journal of Aeronautical Sciences*, Vol. 25, No. 2, 1958.

70.Gnoffo, P. A., "An Upwind-Biased, Point-Implicit Relaxation Algorithm for Viscous Compressible Perfect Gas Flows," NASA TP 2953, Feb., 1990.

71.Cheatwood, F. M., and Gnoffo, P. A., "User's Manual for the Langley Aerothermodynamic Upwind Relaxation Algorithm (LAURA)," NASA TM 4674, April, 1996.

72.Baldwin, B. S. and Lomax, H., "Thin Layer Approximation and Algebraic Model for Separated Turbulent Flow," AIAA Paper 78-257, Jan. 1978.

73.Cheatwood, F. M., and Thompson, R. A., "The Addition of Algebraic Turbulence Modeling to Program LAURA," NASA TM-107758, April 1993.

74.Dhawan. S., and Narashima, R., "Some Properties of Boundary Layer Flow from Laminar to Turbulent Motion," *Journal of Fluid Mechanics*, Vol. 1, Part 4, Jan. 1958, pp. 418-436.

75.Thomas, J., Krist, S., and Anderson, W., "Navier-Stokes Computations of Vortical Flows Over Low Aspect-Ratio Wings," *AIAA Journal*, Vol. 28, 1990, pp. 205.

76.Krist, S., Biedron, R. T., and Rumsey, C. L. CFL3D User's Manual (version 5) Sept. 1997. (see also http://fmad-www.larc.nasa.gov:80/~biedron/ Cfl3dv6/cfl3dv6.html for Version 6 information).

77.Roe, P. "Approximate Riemann Solvers, Parameter Vectors, and Difference Schemes," *J. Computational Phys*. Vol. 43, PP. 357, 1981.

78. Chang, C.-L., "The Langley Stability and Transition Analysis Code (LASTRAC) – Part 1 LST, Linear and Nonlinear PSE for 2D, Axisymmetric and Infinite Swept Wing Boundary Layers, Proposed NASA TM, 2002.

79. Malik, M. R., and Spall, R. E., "On the Stability of Compressible Flow past Axisymmetric Bodies," *J. Fluid Mechanics*, Vol. 228, pp. 443-463, 1991.

80.Pate, S. R., "Dominance of Radiated Aerodynamic Noise on Boundary –Layer Transition in Supersonic-Hypersonic Wind Tunnels," AEDC-TR-77-107, March, 1978.

81.Demetriades, A., "Comparison of Techniques for Defining the Transitional Region Extent," 5th NASP Transition Workshop, NASA LaRC, Feb., 1992.

82.Zanchetta, M. A., and Hillier, R., "Blunt Cone Transition at Hypersonic Speeds: The Transition Reversal Regime," *Proceedings of the colloquium on Transitional Boundary Layers in Aeronautics*, Amsterdam,Dec., 1995, pp. 433-440.

83.Mack, L. M., "Stability of Axisymmetric Boundary Layers on Sharp Cones at Hypersonic Mach Numbers," AIAA Paper 87-1413, June 1987.

84.Malik, M R., "Prediction and control of Transition in Supersonic and Hypersonic Boundary Layers," *AIAA Journal*, Vol. 27, No. 11, Nov., 1989, pp. 1487-1493.

85.Bertin, J. J., *Hypersonic Aerothermodynamics*, edited by J. S. Przemieniecki,, AIAA Educational Series, AIAA, Washington, DC, 1994, pp. 373-395.

86.Schneider, S. P., "Flight Data for Boundary-Layer Transition at Hypersonic and Supersonic Speeds," *Journal of Spacecraft and Rockets*, Vol. 36, No. 1, 1999, pp. 8-20.

87.Chang, C. -L., "Non-Parallel Stability of compressible Boundary Layers," AIAA Paper 93-2912, 1993.

88. Stetson, K. F., Thompson, E. R., and Donaldson, J. C., "Boundary-Layer Stability on a Cones at Mach 8," AIAA Paper 83-1761, 1983.

89.Chang, C. -L., Malik, M R., Erlebacher, G. and Hussaini, M. Y.," Compressible Stability of Growing Boundary Layers Using Parabolized Stability Equations," AIAA Paper 91-1636, 1991.

TABLE 1. Flow Conditions for the NASA LaRC 20-Inch Mach 6 Air Wind Tunnel.

Re_∞/ft ($x10^6$)	M_∞	P_0(psia)	T_0(°F)
1.1	5.9	63	421
2.2	5.9	124	450
2.8	5.9	131	352
2.8	5.9	156	445
3.2	6.0	182	444
4.3	6.0	257	445
5.4	6.0	326	472
6.2	6.0	372	470
7.8	6.0	476	475

Shaded conditions represent a match to Mach 6 NTC Quiet Tunnel reservoir conditions

TABLE 2. N-factor values correlated with measured transition onset on the flared cone.

Re_∞/ft ($x10^6$)	x_T (in.)	N (LST)	N (PSE)
2.2	14	3.0	4.0
2.8	12.25	3.8	6.4
2.8 (cold wall)	12.25	4.5	6.3
4.3	7.5	3.5	5.9
6.2	6.0	4.0	6.5